X-ray Luminosity Function of Optically Selected Galaxy Groups

By

Cai Wood

Faculty of Science

University of Bristol

A dissertation submitted to the University of Bristol in accordance with the requirements of the degree of Master of Science in the Faculty of Science.

January 9, 2020

Word count: 17,051

Abstract

The Galaxy and Mass Assembly (GAMA) spectroscopic survey consists of roughly 300,000 galaxies covering 286 deg^2 down to an r-band magnitude of 19.8. A 16.6 deg^2 area of the GAMA survey overlaps with the XXL survey, which is the largest homogeneous survey carried out with *XMM-Newton* to date. The overlap between the GAMA optical survey and the XXL X-ray survey creates an exciting opportunity to explore galaxy groups across multiple wavelengths with independent selection criteria. This overlap region contains 234 galaxy groups with five or more members detected by GAMA. The XXL X-ray mosaic created by combining multiple *XMM-Newton* observations is used to determine the X-ray luminosity of GAMA's optically selected sample of galaxy groups. Forced X-ray aperture photometry was used, with emission from AGN and other non-group X-ray sources modelled out or removed, and then luminosity posteriors were sampled to deal with non-detections. This sample of galaxy groups are then presented as an X-ray luminosity function (XLF): the number density of groups as a function of X-ray luminosity. Due to the optical selection criteria used the XLF is able to explore lower X-ray luminosities than X-ray selected samples could. However, incompleteness from the optical selection function only including groups with five or more members results in a lower luminosity limit of 1.9×10^{40} erg s^{-1} being implemented in the XLF fitting. The XLF demonstrates that the Schechter function remains a good description down to lower-luminosities and for an optically selected sample which has different biases than an X-ray selected sample. The Schechter function best fit parameters observed are consistent with values determined using X-ray selected samples. The issue of incompleteness due to the optical selection function needs to be further explored, and by combining the observed XLF with a theoretical mass function this work will ultimately lead to new constraints on the scaling relation between X-ray luminosity and mass in the galaxy group regime.

Dedication and acknowledgements

First and foremost I would like to thank my supervisor Dr. Ben Maughan for his guidance, discussions, support, reassurance and enthusiasm throughout this project. His subject knowledge is first rate and his organisational skills kept me on track throughout my research. I would also like to thank Dr. Rhys Morris for his training and ongoing assistance with the Linux systems. Finally I would like to thank all my fellow postgraduate students, family and friends for their ongoing support and assistance throughout this project.

Author's declaration

I declare that the work in this dissertation was carried out in accordance with the requirements of the University's Regulations and Code of Practice for Research Degree Programmes and that it has not been submitted for any other academic award. Except where indicated by specific reference in the text, the work is the candidate's own work. Work done in collaboration with, or with the assistance of, others, is indicated as such. Any views expressed in the dissertation are those of the author.

SIGNED: .....Cai Wood..... DATE: .....September 13, 2019.....

Contents

List of Tables

List of Figures

1 Introduction

Cosmology is the study of the origin and evolution of the Universe, and as such requires a full view of the Universe. Since galaxy clusters are the largest gravitationally bound objects in the Universe, they are ideal candidates with which to study cosmology.

1.1 Cosmology

The foundation of cosmology is the cosmological principle, which states that on large scales the Universe appears homogeneous and isotropic. This builds on Einstein's theory of general relativity, where gravity is a manifestation of the curvature of space-time.

1.1.1 Hubble's law

Hubble's law first introduced the theory that the Universe is expanding, and this expansion rate is calculable. This expansion can be observed through the redshift (z) of photons. Redshift is a measure of the expansion of space between the location of emission and observation, given by

$$1 + z = \frac{\lambda_{obs}}{\lambda_{em}} \tag{1}$$

where λ_{em} and λ_{obs} are the photons' wavelength when emitted and observed.

Hubble's law states that the recession velocity (v) of an object is linearly proportional to its proper distance (D), with the constant of proportionality being the Hubble constant, H_0. The Hubble constant is the observable value of the Hubble parameter (H) at the current time and as such is the expansion rate of the Universe today. The evolution of the Hubble parameter is given as

$$H(z)^2 = H_0^2 E(z)^2 \tag{2}$$

where

$$E(z)^2 = \Omega_R(1+z)^4 + \Omega_M(1+z)^3 + \Omega_\Lambda + (1-\Omega_0)(1+z)^2 \tag{3}$$

with Ω_M, Ω_R and Ω_Λ being the matter, radiation and dark energy density parameters of the Universe, with Ω_0, their sum, describing the curvature of the Universe.

This work assumes the WMAP9 cosmology from Hinshaw et al. (2013) with $\Omega_M = 0.2815$, $\Omega_R = 0$ and $\Omega_\Lambda = 0.7185$. This describes a flat Λ cold dark matter (ΛCDM) cosmology, whereby the Universe is currently made up of dark energy, dark matter and baryonic matter.

1.1.2 Distances and volume

Due to the non-linear nature of the expansion of the Universe, there are multiple possible definitions of distance, for this work only four will be discussed. The first, and most intuitive, is the proper distance, d, which increases as the Universe expands. The comoving distance, χ, is the distance between objects on an expanding coordinate system. As such, χ remains constant as the Universe expands, and is related to d via the scale factor, $a(t)$, which describes the scale of the Universe as a function of time. Differentiating χ and substituting the proper distance returns Hubble's law, since the Hubble parameter is the change in scale per unit scale.

Being able to determine the distances from a physical observable such as the redshift is useful for astrophysics, and having such a relationship allows the constraining of cosmological parameters

by comparing different methods. Consider a photon emitted at t_e and observed at t_0, in this time the Universe will have expanded by a factor $a_0/a(t_e)$, and the wavelength of the photon will have been stretched by the same factor. In a time interval dt the photon travels a proper distance cdt, thus the total proper distance traversed is its integral. Since comoving distance is the proper distance divided by the scale factor, and the relationship between the scale factor and redshift is known, the comoving distance travelled by the photon is given by

$$\chi = \frac{c}{a_0 H_0} \int_0^z \frac{dz}{E(z)}. \tag{4}$$

The next distance is termed the luminosity distance, d_L. To explain d_L, consider the flux (f) observed from a source luminosity L at proper distance d in a non-expanding Universe:

$$F = \frac{L}{4\pi d_L^2}. \tag{5}$$

In an expanding Universe, the incoming flux is decreased by a factor of $1 + z$ due to the redshift from the expansion of the Universe, and another factor of $1 + z$ from the time dilation between the source and observer. Both effects reduce the flux by $(1 + z)^2$, and this means that

$$d_L = (1 + z)d = \sqrt{\frac{L}{4\pi F}}. \tag{6}$$

The final distance is the angular diameter distance, d_A. In a flat non-expanding Universe the physical size (D) divided by the angular size (θ) returns the distance. In an expanding Universe this would be the proper distance when the photons are emitted. In the time taken for the light to travel to the observer, the Universe is larger by a factor $1 + z$, and thus

$$d_A = \frac{D}{\theta} = \frac{d}{1 + z}. \tag{7}$$

Since these distances are all linked, knowing one implies knowledge of all. Therefore if the recession velocity, or redshift, of an object is known then its distance can be calculated for a given cosmology. For a detailed discussion on calculating these distances see Hogg (1999).

Similarly to distances, due to the expanding nature of the Universe there are multiple definitions for the volume of space, however, the most cosmologically useful one is the comoving volume. This can be considered as the volume found using an expanding coordinate system such that the number densities of non-evolving objects, whose motion is solely due to the expansion of the Universe, are constant with redshift. Consider a proper volume element of the Universe subtending a solid angle $d\Omega$ over a redshift range dz. The angular diameter distance squared is used to convert a solid angle into a proper area, and then apply Equation 6 to obtain a comoving area. Multiplying this by the comoving distance element from Equation 4, the comoving volume element dV is given by

$$dV = \frac{c}{a_0 H_0} \frac{(1 + z)^2 d_A^2}{E(z)} d\Omega dz. \tag{8}$$

1.1.3 Critical density

The Universe is expanding at a rate measured by the Hubble parameter, and this expansion is being counteracted by the force of gravity, which is trying to close the Universe. This gives

three possibilities for the shape of the Universe, Open, closed or flat, which correspond to the Universe expanding forever, collapsing down or expanding at an ever slower rate until expansion halts after an infinite time. Since the current best estimate for the cosmological model of the Universe involves a flat curvature, the density of the Universe must be at a certain value whereby the Universes expansion is halted after an infinite time, called the critical density. The critical density as a function of redshift is given by

$$\rho_{crit}(z) = \frac{3H_0^2}{8\pi G}E(z)^2, \tag{9}$$

where G is the gravitational constant.

1.2 Galaxy clusters

Towards the end of the 18th century the clustering of nebulae was noticed, however, it wasn't until the 20th century that these nebulae where demonstrated to be external galaxies. Zwicky (1933) determined that galaxy clusters must be more than a collection of galaxies when he discovered that 400 times the total mass from galaxies is required for the Coma cluster to be stable. Zwicky was able to measure the cluster mass by applying the virial theorem to the observable velocity distribution. With this he introduced the first evidence for dark matter. Following this the first optically selected catalogue of galaxy clusters was determined by Abell (1958) and used to study the richness and morphology of clusters. Clusters are detected in the optical based on over-densities of galaxies, however, this does suffer from projection effects due to foreground and background galaxies. The next step in galaxy cluster science came when the first X-ray satellites where launched in the 1960s, and started to detect X-ray emission from regions around bright galaxies in the centres of nearby groups. Over then next decade it was suggested that galaxy clusters are X-ray sources, and this was confirmed by the Uhuru catalogue of X-ray sources (Giacconi et al., 1972). It was found that the X-ray emission originated from a hot, diffuse, ionised plasma called the intracluster medium (ICM). The gravitational potential well of a galaxy cluster compresses and heats up in-falling ICM to temperatures of around 10^7K, which emits in the X-ray part of the spectrum. The primary emission mechanism is thermal Bremsstrahlung and was first suggested by Felten et al. (1966). The X-ray luminosity due to Bremsstrahlung is related to the ICM density (ρ), volume (V) and temperature (T) with the form

$$L_x = \rho^2 V T^{\frac{1}{2}}, \tag{10}$$

where we assume a linear relation between the electron, ion and ICM densities (Mushotzky, 1984; Sarazin, 1986). There are also weak contributions by two other continuum emission mechanisms: free-bound emission and two-photon emission (Kaastra et al., 2008). Aside from continuum emission, line radiation is also visible in X-ray spectra from the excitation and emission processes of ions. The ICM is also detectable in the radio through the Sunyaev-Zel'dovich (SZ) effect. This is the temperature change of the cosmic microwave background photons due to inverse compton scattering as they traverse the ICM. Since the SZ effect is a scattering effect its signal to noise is independent of redshift as opposed to most other detection techniques.

Today, we know that galaxy clusters are dark matter haloes with an assembly of galaxies confined within a common gravitational potential well. Their formation traces back to the early Universe which was smooth with small density perturbations. These were then amplified by gravity as time went on, eventually collapsing and merging to form galaxy clusters in a process called

hierarchical formation. Galaxy clusters and groups are not distinct classes, however, they are conventionally differentiated based on the number of galaxies within them, with groups typically having fewer than ten galaxies. Between 5% and 20% of the mass of a galaxy cluster is made up of baryonic matter, with the rest being invisible non-baryonic dark matter (White et al., 1993). About 85% of the baryonic matter is made up of the ICM with the remainder being from stars, dust and cold gas. For reviews of cosmological results obtained from observations of galaxy clusters see Allen, Evrard & Mantz (2011), Vikhlinin et al. (2014) and Pratt et al. (2019).

1.2.1 The β-model

The observed X-ray surface brightness profiles from the ICM for a wide range of galaxy groups is well described by a β-model. The β-model approximates the group emission as an isothermal sphere, and as such the brightness (I) as a function of projected radius (x) is given by (Jones & Forman, 1984):

$$I(x) = I_0 \left[1 + \left(\frac{x}{r_c}\right)^2\right]^{-3\beta+\frac{1}{2}}, \tag{11}$$

where r_c is the core radius, which sets the radial scale of the core region (discussed in Section 2.4.3), and β mathematically determines the slope of the surface brightness profile at large radii. β is also physically defined to be the ratio of specific energy in the galaxies to that in the ICM, and is commonly set to be two-thirds. Not only was this roughly the value found by Mohr, Mathiesen & Evrard (1999), but it also results in being able to analytically solve the integral of the β-model. This analytical solution is useful as it allows for an aperture correction, which finds the ratio of flux within an aperture size x to total flux using:

$$\frac{\int_0^\infty I(x)dx}{\int_0^x I(x)dx} = \frac{\sqrt{r_c^2 + x^2}}{x}. \tag{12}$$

1.2.2 Self-similarity in galaxy clusters

The hierarchical formation model suggests that since galaxy clusters form via mergers, provided the changing density of the Universe is accounted for, then all clusters should be identical, scaled versions of each other. With these assumptions of self-similarity (Kaiser, 1986), power-law shaped scaling relations between galaxy cluster properties (such as luminosity, mass and temperature) can be derived.

Of great astrophysical interest is the luminosity-mass (LM) relation which relates a directly observable property of the cluster with one that is not possible to observe directly. The LM relation follows the form given by Maughan (2007):

$$L_X = CE(z)^\alpha \left(\frac{M}{M_*}\right)^B, \tag{13}$$

where C (in units 10^{44} erg s^{-1}) and B are the power-law normalisation and slope, α is 7/3 for self similar evolution and M_* is $4 \times 10^{14} M_\odot$. Studies done to date on the LM relation typically find slopes steeper than expected under the assumption of self-similarity (Maughan, 2007; Giodini et al., 2013; Wang et al., 2014; De Martino & Atrio-Barandela, 2016). Discussion as to the origin of this discrepancy is ongoing, with contributions attributed to non-gravitational heating and a break in the LM relation towards low mass systems (Anderson et al., 2015; Lovisari, Reiprich &

Schellenberger, 2015). Due to the difficulty in obtaining data for low mass groups the LM relation of low mass groups has yet to be systematically studied. Future work done using an optically selected group sample, whose mass range extends far lower than an X-ray selected group sample, will allow the exploration of the low mass and low X-Ray luminosity regime of the LM relation. Exploring the form of the LM relation at low masses is interesting as it encodes information about feedback in clusters that has affected the ICM over time.

1.3 The X-ray observatory *XMM-Newton*

The X-ray Multi-Mirror (XMM) Newton satellite was launched by the European Space Agency in December 1999. *XMM-Newton* consists of three X-ray telescopes each with 58 Wolter mirrors giving a large effective area of 0.4 m^2 which is captured using the European Photon Imaging Camera (EPIC). This consists of one EPIC-PN BI CCD camera and two EPIC Metal Oxide Semiconductor (MOS) FI CCD cameras with gratings. *XMM-Newton* has the largest effective area of any focusing X-ray telescope, thus making it ideal for galaxy cluster surveys.

The background counts detected by *XMM-Newton* has a cosmic particle X-ray background component and an instrument background component (Pierre et al., 2016). The instrument background is low in the 0.5-2.0 keV energy band since its two components, detector noise and particle-structure interactions, are most dominant below 200 eV and above 2 keV respectively. However, the instrument background contains a flaring component which is attributed to soft photons and is characterised by strong and rapid variability.

A significant fraction of the data is contaminated by solar proton flares, especially when *XMM-Newton* passes near the Van Allen radiation belt. The effects of flares is twofold, firstly, the filtering results in a reduced effective observing time and secondly, the background in the remaining observation is often elevated.

1.3.1 The PSF

The point spread function (PSF) describes the spatial resolution of the telescope as a probability distribution of detection from a point source. The PSF of an X-ray telescope is energy and position dependent, and is also not azimuthally symmetric. The three X-ray telescopes used on *XMM-Newton* have different PSFs which do, however, all share some similarities, primarily the radial substructures, 'spokes', caused by the spiders holding the mirror shells. While a PSF correction is important if the source region is small compared to the PSF, it is often not required for extended emission. For a more detailed explanation about the *XMM-Newton* PSF see Read et al. (2011).

For this work the PSF was required for the removal of emission from point sources near, or in, the group emission. To obtain a reasonable PSF for use with the XXL field data, an observation taken roughly halfway through the XXL data gathering stage is used. This gives a reasonable estimate of the PSF whilst taking into account its degeneration over time. The observation used was Obs.ID 0037980101 taken on January the 11th 2002, downloaded from the *XMM-Newton* Science Archive. This is a 15ks observation taken in the north XXL field, and in order to obtain a PSF the ESA Science Analysis System (SAS) is used. The observation was processed, and the PSF obtained using the current best model, called ELLBETA, which includes instrument distortions and the 'spokes'. The PSF used can be seen in Figure 1, and corresponds to the on-axis position of the MOS1 camera for an energy of 1keV. The shape of the PSF at off-axis positions becomes elongated due to off-axis aberration. The data used is built up of many overlapping pointings and

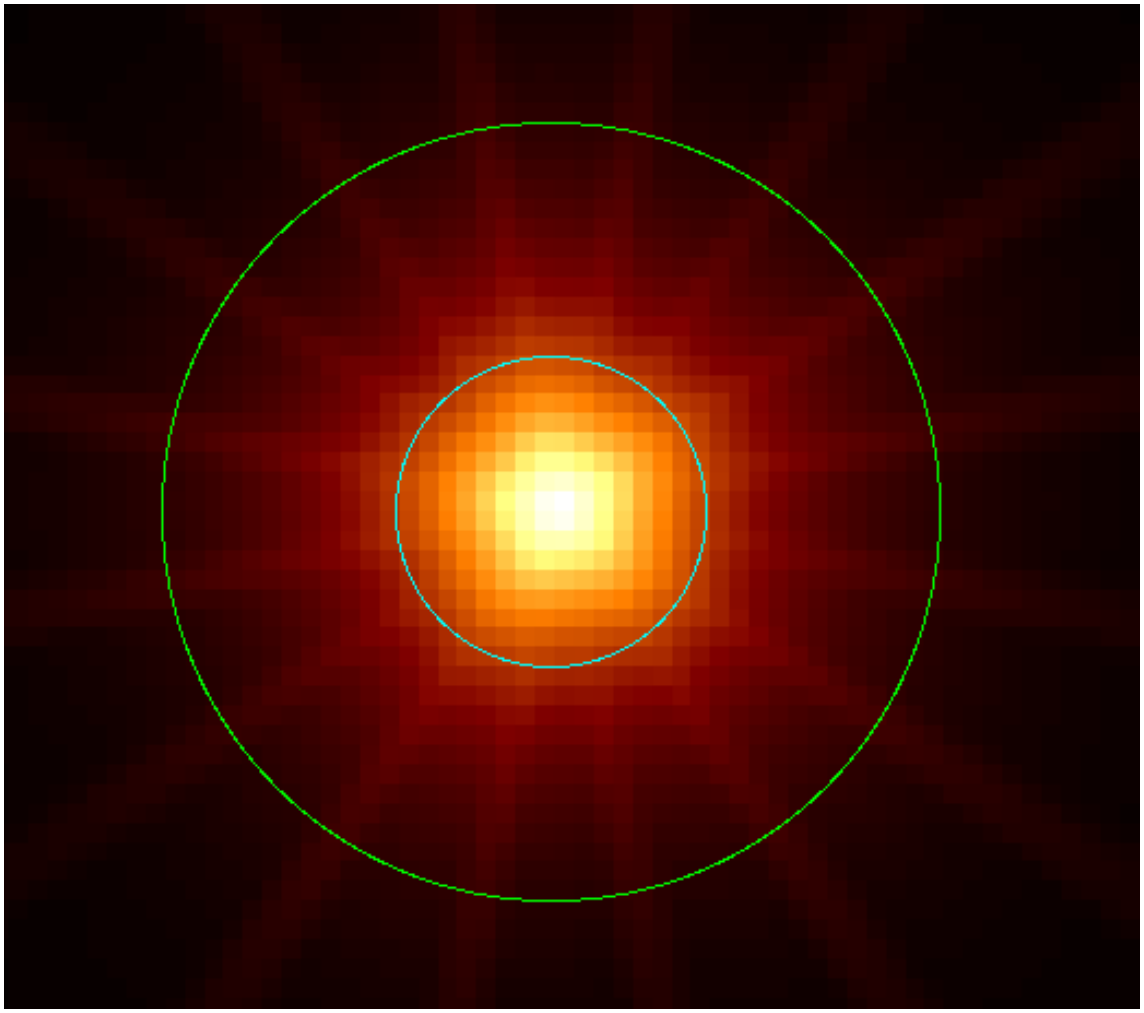

Figure 1: The *XXM-Newton* PSF used for this project, with the blue and green circles representing 20" and 50" radii which hold 75% and 90% of the light respectively. This agrees with the values shown by Read et al. (2011).

the most off-axis position an object can be from the closest axis is only 10', which for low-energy emission only results in a 6% increase in the radius of the PSF which encloses 90% of the total energy. The overlapping regions means that the PSF can have contributions from many different pointings, resulting in multiple different shape changes. Rather than attempt to model all these minimal effects, it is reasonable to use the on-axis PSF and assume the off-axis effects are negligible.

1.4 Galaxy cluster surveys

In order to determine the characteristics and abundances of galaxy clusters (and groups) it is necessary to catalogue statistically complete samples. The results obtained from analysing the samples can then be compared to cosmological models to determine number density functions and scaling relation laws for observable and non-observable parameters. In order to detect galaxy groups in X-ray, the ICM must be observed, and as such must be bright enough to be detectable above the background, and extended enough to be classified as an extended source. X-ray selected cluster surveys are currently the most statistically well defined, and due to the X-ray luminosity being proportional to the ICM density squared, they are far less biased due to projection effects

than their optical counterparts. X-ray selected clusters are also more likely to be evolved, since a deep gravitational potential well is required for bright X-ray emission.

The two original galaxy cluster catalogues are those of Abell (1958) and Zwicky et al. (1961) and both where constructed by counting over densities of galaxies. The earliest reasonably complete catalogue by de Vaucouleurs (1975) was reconstructed by Huchra & Geller (1982) using a quantitative method to create the first reproducible cluster catalogue based on galactic positions and redshifts. More recently the fact that galaxies located in the cores of galaxy clusters have older stellar populations, and so form a tight red-sequence in colour magnitude space led Gladders & Yee (2000) to create a red-sequence based cluster finding algorithm which was applied in the construction of the first Red-sequence Cluster Survey by Gladders & Yee (2005). This work was expanded by Koester et al. (2007) and Yang et al. (2007) using the Sloan Digital Sky Survey to detect galaxy clusters based on their brightest cluster galaxy and location in position and redshift space.

While the largest cluster catalogues to date have been constructed using optical data, X-ray constructed surveys are increasing in popularity, especially with the launch of *ROSAT* in the 1990s. The *ROSAT* All-Sky Survey by Truemper (1993) is the only all-sky survey conducted using an imaging X-ray telescope and provided the foundation for the largest, high-quality X-ray selected sample of galaxy clusters by Böhringer et al. (2004), which was extended to create the REFLEX II cluster sample (Böhringer et al., 2013). *ROSAT* was also used for many serendipitous X-ray cluster surveys such as the 400 square degree survey (Vikhlinin et al., 1998a; Burenin et al., 2007) and the Wide Angle *ROSAT* Pointed Survey (Horner et al., 2008, WARPS). *XMM-Newton* and *Chandra* have also been used for serendipitous cluster detections by the XMM Cluster Survey (Mehrtens et al., 2012) and the *Chandra* Multiwavelength Project (Barkhouse et al., 2006) respectively. Cluster surveys are also carried out in the millimetre using the SZ effect, such as the South Pole Telescope Survey (Reichardt et al., 2013) and the all-sky Planck (Ade et al., 2016), and due to the redshift independent nature of their detection, are likely to be the primary method for future cluster surveys.

1.4.1 Selection bias

Clusters are typically selected if their flux is above a survey flux limit. This flux limit is in fact a surface brightness limit, and so unless the detection method accounts for this, very diffuse and extended clusters can be passed due to the surface brightness within an aperture not passing the flux limit, despite the cluster itself having a high enough flux. However, X-ray surveys are biased towards more X-ray luminous clusters, since they operate using a minimum flux cutoff, and as such for any given cluster mass the luminosity will be overestimated. To attempt to correct for this bias, a statistically complete optically selected sample of galaxy clusters can be used, which is not dependent on the X-ray luminosity. This allows the characterisation of low X-ray luminosity groups, which would otherwise not have passed the threshold for X-ray detection.

A wavelength independent detection bias is the Malmquist bias which arises because brighter objects can be seen over greater distances, and as such high luminosity objects have a larger survey volume. This is solved for by using a selection function which determines the volume at which each object could be detected, and then doing any statistical work using number densities. Another bias is the Eddington bias which occurs due to the statistical fluctuations in measurements and plays an important role when using detection thresholds. If an observable, such as luminosity, follows a

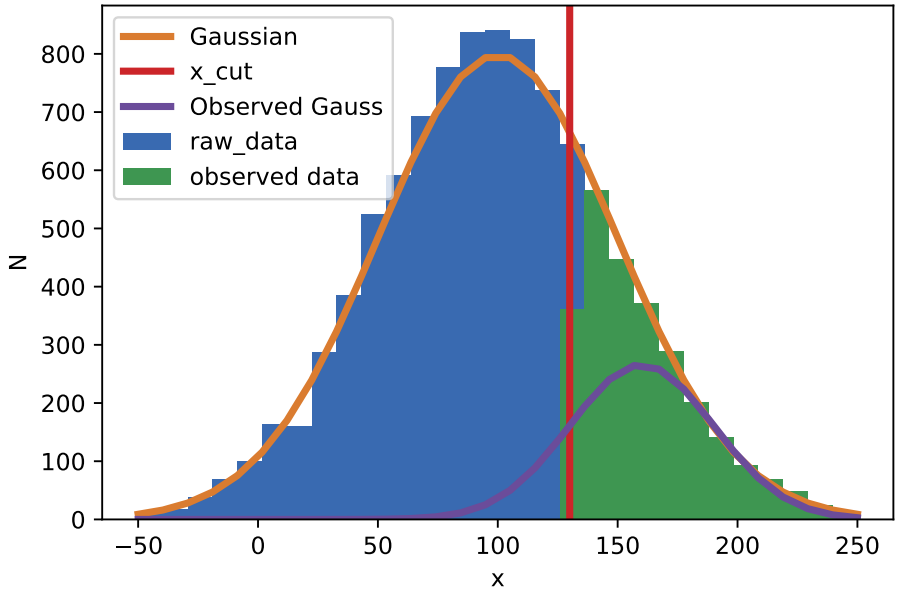

Figure 2: A normal distribution with mean 100 and standard deviation of 50 shown in orange which is sampled to give the raw data shown in blue. The cut used to represent the selection effect is at 130 in red, resulting in an observed sample shown in green, from which the mean and standard deviation produce the purple normal distribution, which is clearly not representative of the raw data.

power law then the number of objects in the bin directly below the detection threshold is far greater than the number above the detection threshold. Since any observable has some intrinsic statistical scatter, the number of objects scattered up from below the threshold is greater than the number of objects scattered down to below the threshold. This results in the number of detected objects above the threshold being increased above their true value. This is accounted for by finding the probability of observing the data given a model, instead of simply fitting a model to the data. For a basic example see Figure 2, which represents a parameter x whose distribution is represented by a normal distribution. When a selection is applied to the data, a simple cut in x in this case, then treating the observed data as the true x would result in an incorrect determination of x, as can be seen. In order to find the true mean and standard deviation for x from the observed data, then the selection function must be accounted for, for a detailed analysis of how to cope with selection effects see Mantz (2019).

A combination of the Malmquist and Eddington bias is also prevalent when comparing two properties if one of them has a threshold, for example when comparing mass and luminosity. Given the Eddington bias, for any given mass there will be a range of possible luminosities, and due to the Malmquist bias, the objects with higher luminosities are more likely to be observed. This threshold results in the objects with lower luminosities for a given mass being missed. This results in the luminosity for any given mass being potentially overestimated, and this is especially important when nearing the luminosity detection threshold.

1.5 The XXL survey

The XXL Survey is a large X-ray survey using XMM-Newton covering two extragalactic areas of $25\,deg^2$ each with a point source sensitivity of $\sim 5 \times 10^{-15}$erg s^{-1} cm^{-2} in the $[0.5-2]\,keV$ band (Pierre et al., 2016). This is the largest XMM programme to date totalling 6.9 Ms. The programmes' main goals are to provide constraints on the dark energy equation of state from the space-time distributions of clusters of galaxies and to serve as a pathfinder for future, wide-area X-ray missions. There are 35 XXL papers published as of January 9, 2020, with four more to be published in the coming months. These cover many topics, but are primarily focused on the study of clusters and AGN. As of December 2015, some 450 new galaxy clusters have been detected out to $z \sim 2$ as well as more than 22,000 Active Galactic Nuclei out to z$\sim$4.

1.5.1 Source detection

The standard spacing between individual XXL pointings is 20' allowing for optimal overlap between observations, given that there is a 50% decrease in effective area at 10'. The clean event lists from the three detectors are combined and then detected using SExtractor (Bertin & Arnouts, 1996) and analysed using Xamin as described in Pacaud et al. (2006). For this process each observation is individually processed and sources are detected within 13' from the centre of the XMM field of view. This leads to off-axis sources being missed or miss-characterised. To solve this the Xamin pipeline is being rewritten by Faccioli et al. (2018) to allow the combined use of all available pointings simultaneously.

To detect groups, the pipeline searches for extended sources, defined as being larger than 5" in extent and having an extension likelihood larger than 15. Further analysis splits the extended sources into two classes, C1 and C2, where C1s are more likely to be clusters since their extension likelihood is greater than 33 and they have a detection likelihood above 32. The flux limit for the XXL galaxy cluster catalogue is 3×10^{-14}erg s^{-1} cm^{-2}, and of the 365 clusters included in the cluster catalogue, 341 have been spectroscopically confirmed (Adami et al., 2018). Of the 365 clusters, only 207 are classified as C1, while 119 C2 and 39 C3 clusters are included by merit of having been spectroscopically confirmed.

1.6 The GAMA survey

The Galaxy and Mass Assembly (Driver et al., 2011, GAMA) spectroscopic survey of 300,000 galaxies covers 286deg^2 down to an r-band magnitude of $r < 19.8$ mag, carried out using the Anglo-Australian Telescope (Davies et al., 2019). The GAMA survey created a GAMA galaxy group catalogue which was generated using a friends-of-friends (FoF) based grouping algorithm. A FoF algorithm links galaxies based on their separation as a measure of the local density, and the GAMA FoF algorithm is run on GAMA survey style mocks to test the quality of the grouping and then run on the real GAMA data for the best results. The overdensity with respect to the mean required to define a group is 0.06 and the mean comoving inter-galaxy separation is found for each galaxy at its position based on the absolute magnitude limit of the survey and the galaxy luminosity function. The mean comoving inter-galaxy separation is multiplied by the overdensity and the radial expansion factor to account for peculiar motions of galaxies within groups, which was found to be 18, and this value compared to the observed inter-galaxy separation. For a detailed description of the FoF algorithm parameters see Robotham et al. (2011), along with other

parameters used to better modify the linking. When tested on the mock data, the GAMA FoF algorithm is able to recover 89% of all groups, and the number of groups detected below a redshift of 0.5 is remarkably consistent between the mocks and real groups (Robotham et al., 2011). The GAMA catalogue includes calculated group parameters for groups with five or more members, however, it was found that groups with fewer than five members where not possible to analyse accurately.

The GAMA survey uses three different methods to determine the location of a galaxy group, which are using the centre of light (CoL) in r_{AB}-band, an iterative procedure using the CoL and using the brightest cluster galaxy (BCG) location. The iterative procedure involved removing the most distant galaxy from the CoL until only two galaxies remain, then the brightest r_{AB}-band of the two is chosen as the group centre and referred to as the IterCen. When compared to the mocks it was found that 95% of the groups with five or more members had the IterCen as the same group as the BCG. A gapper estimator is used to measure the group velocity dispersion (σ) which in turn is used to determine each groups mass. The gapper estimator orders the recession velocities, and then calculates the sum of the weighted gaps between each velocity pair and then normalises based on the number of galaxies. This is corrected for the uncertainty of the recession velocities by removing the total measurement error in quadrature, for full details see Robotham et al. (2011). The typical error on σ is 50 km s^{-1} and when compared to the mocks 80.4% (50%) of the σ values are within 50% (14%) of the intrinsic value (Robotham et al., 2011).

1.7 X-ray luminosity function

The X-ray luminosity function (XLF) is used to summarise and compare properties of statistically complete samples of luminous objects, and is defined as the comoving number density (n) per luminosity interval. This is mathematically described using the Schechter function (Schechter, 1976):

$$n(L_x)dL_x = n^* \left(\frac{L_x}{L^*}\right)^{-\alpha} \exp\left(\frac{-L_x}{L^*}\right)\frac{dL_x}{L^*} \tag{14}$$

where n^* normalises the XLF and α determines the power law slope when the galaxy group luminosity (L_x) is less than L^*. The shape of the Schechter function is a power law for low luminosity objects, and an exponential for higher luminosity objects. The selection function is of vital importance when calculating the XLF in order to properly account for survey limitations and potential sources of bias.

The XLF allows for the study of the development of structure, luminosity density and number density in the Universe, and as such has a strong history (Bahcall, 1979; Piccinotti et al., 1982; Vikhlinin et al., 1998b; Allen et al., 2003; Mullis et al., 2004; Koens et al., 2013; Böhringer, Chon & Collins, 2014). Mullis et al. (2004) used the XLF to find significant evidence for negative evolution at the bright end, implying that the number density of high luminosity clusters was lower at high redshifts than in the local Universe. This negative evolution was also observed by Koens et al. (2013) and Adami et al. (2018).

The XLF for the local Universe has also been well studied using *ROSAT* to measure the cluster mass function and hence constrain cosmological parameters (Mantz et al., 2008; Böhringer, Chon & Collins, 2014). A large limitation in the determination of the XLF is the flux limitation of X-ray surveys resulting in the faint end being poorly constrained.

The REFLEX II survey gives a precise XLF for nearby and bright clusters, and surveys such

Survey	Number	L_{min}	n^*	α	L^*
WARPS	124	0.01	3.68 ± 0.87	1.79 ± 0.04	2.59 ± 0.35
REFLEX II	802	0.0019	5	1.74 ± 0.05	1.88 ± 0.20

Table 1: The best fitting XLF parameters found by Koens et al. (2013) and Böhringer, Chon & Collins (2014). n^* is quoted in units of $10^{-7}Mpc^{-3}$ while L_{min} and L^* in units of 10^{44} erg s^{-1}

as WARPS are able to contribute to higher redshifts to test evolution. These surveys are limited by the flux limit of the survey (REFLEX II: 1.8 $\times 10^{-12}$erg s^{-1} cm^{-2} [0.1-2.4keV] and WARPS: 3.5 $\times 10^{-14}$erg s^{-1} cm^{-2} [0.5-2.0keV]) and biased since higher luminosity groups are more likely to be detected.

The work presented here takes advantage of the overlap between the optically selected cluster survey conducted by GAMA, discussed in Section 1.6, and the X-ray selected cluster survey by XXL, discussed in Section 1.5. As this work studies the X-ray properties of galaxy clusters, analytical comparisons will only be made to work done using the X-ray cluster surveys done by the extended *ROSAT*-ESO Flux Limited X-ray Galaxy Cluster Survey (REFLEX II) and the Wide Angle *ROSAT* Pointed Survey (WARPS). Since the REFLEX II luminosities were all determined in the 0.1-2.4 keV energy band, whereas the XXL and WARPS luminosities are in 0.5-2.0 keV, all REFLEX II values must be corrected. This correction factor was determined to be in the range 0.60-0.65 depending on the cluster temperature, and since Böhringer, Chon & Collins (2014) determined the REFLEX II flux limit based on a cluster with temperature 5keV, the correction was determined at this temperature to be 0.62. All REFLEX II values shown in this work have been corrected to be in the 0.5 - 2.0 keV energy band unless stated otherwise. These XLFs where chosen as comparisons since they produced the two most recent works detailing the X-ray luminosity function, see Koens et al. (2013) and Böhringer, Chon & Collins (2014). Adami et al. (2018) give a XLF which was computed based on a luminosity-temperature. However, this XLF has not been fit using a Schechter function or similar and so this work is unable to compare the results analytically. Since this work uses the XXL data, comparing the shape of the XLF computed by Adami et al. (2018) provides a useful comparison since the high end luminosities should in theory match.

1.8 Outline of this study

This thesis uses the overlap between the GAMA survey and the XXL survey to study the X-ray properties of optically selected galaxy clusters. This removes X-ray selection biases from the sample, particularly in that no groups are lost due to having a low surface brightness or being miss identified as AGN. Since the selection function used is not directly dependant on the group X-ray luminosity, and does not have an X-ray flux limit, this work extends to lower luminosities than previously determined XLFs. Since the majority of the galaxy clusters discussed in this work have less than ten members, from this point onwards all galaxy clusters and groups will be referred to solely as groups.

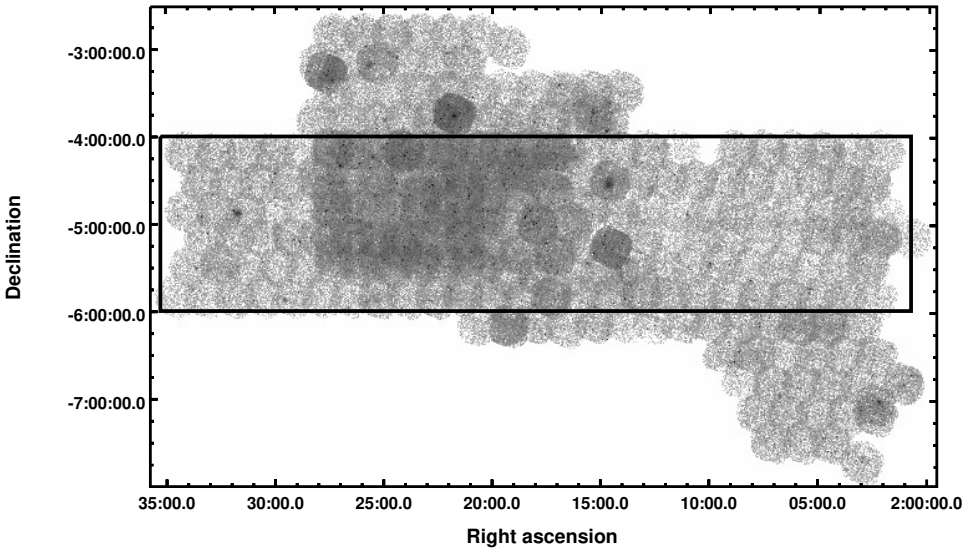

Figure 3: The count rate map of the XXL-N field, with the box highlighting the region used to select GAMA groups.

2 Galaxy Group Sample

The latest GAMA FoF galaxy group catalogue, G^3Cv10, contains 26,194 galaxy groups with at least two members. This number is narrowed down to only include groups with five or more members, which have properties which are in good agreement with the mock catalogues as explained by Robotham et al. (2011). This results in a list of 3061 GAMA selected galaxy groups, which is further reduced by selecting groups found only in the overlap between the XXL and GAMA surveys. This is initially set as being within RA = 30.2 - 38.8 and Dec = -4.0 - -6.0 deg. As seen in Figure 3 this includes regions without XXL pointings, and as such any GAMA groups whose location didn't lie within an XXL tile were also removed. This resulted in 234 GAMA groups within a total solid angle of 16.6 deg^2, which is the total solid angle for which XXL had exposure time within the GAMA overlap region. For this work it is assumed that all groups with five or more members are indeed a group, and not random. There is a trade-off between purity and number, and Robotham et al. (2011) found that groups with five or more members have a very high level of purity, and whilst including groups with fewer than five members would increase the number, the decrease in purity would be large.

Finally, for the purpose of this work, the selection function is such that the fifth brightest galaxy in a group must have an apparent magnitude greater than -19.8, and must be located within the 16.6 deg^2 GAMA XXL overlap region.

2.1 Survey volume for each group

Since the selection criteria for inclusion of a galaxy group required at least five galaxies, the magnitude of the fifth brightest galaxy in every group can be used to determine the maximum distance at which the group could be observed. The constituent 2125 GAMA observed galaxies for the 234 GAMA groups analysed all have observed redshifts and apparent r-band magnitudes. From the redshifts, each galaxy's luminosity distance is determined, and thus the absolute magnitude of each galaxy calculated.

Description	Number of GAMA groups
Total GAMA groups	26,194
GAMA groups with 5+ members	3061
GAMA XXL group sample used	234
GAMA groups with XXL group matched	53
GAMA groups with nearby X-ray point sources	142

Table 2: The number of GAMA groups used along with different matching criteria according to nearby galaxy groups or X-ray point sources.

The distance at which the fifth brightest galaxy in a given group would have an apparent magnitude of 19.8 is considered the maximum distance at which that group could have been detected. The redshift at this distance, along with the survey solid angle, is used to find the maximum comoving volume within which this group could be detected, and this V_{max} value is then found for all groups.

2.2 Sample incompleteness

Whilst the method used to obtain the group sample removes some sources of bias and incompleteness, others are introduced. The most major incompleteness introduced is due to selecting only groups with five or more member galaxies. This means that due to scatter between the luminosity and richness, for a given luminosity bin there will be groups with four member galaxies whose luminosity would be within the bin that are missing due to the optical selection function used. This will result in the underestimation of the number density of groups, and since groups with four members are likely to be smaller this will effect the lower luminosity bins more. Accounting for this incompleteness is discussed in Section 4.4, however, when fitting the XLF a first order correction is applied. This correction is to only fit for luminosity bins above $10^{40.9}$ erg s^{-1}, with this value being the estimated mean luminosity of groups with four members, as discussed in Section 4.4.

2.3 Matching with other sources

Since the GAMA group sample is optically selected, it makes sense to check if any of the GAMA groups match groups detected by XXL. This allows a check on the observed luminosities and locations, and to observe inconsistencies between the X-ray and optical samples. Also matching the GAMA groups with XXL detected AGN, along with other non-group X-ray sources allows for the detection and removal of sources of contamination. The process of matching with X-ray sources and determining the X-ray luminosity of each group is summarised in Figure 4 and discussed in detail here, and the resulting number of groups in each category is displayed in Table 2.

2.3.1 XXL detected galaxy groups

A catalogue containing the X-ray luminosities, group classification and positions of the 365 brightest galaxy groups detected by XXL have been published by Adami et al. (2018). To match a GAMA group with an XXL detected group, each GAMA detected galaxy that is a member of a GAMA group is matched with the XXL group catalogue of both group classifications and any XXL group which is located within 120" and a redshift of 0.01 from a GAMA detected galaxy is considered a match. This results in 57 matches, and changing the separation radius to 60" reduces

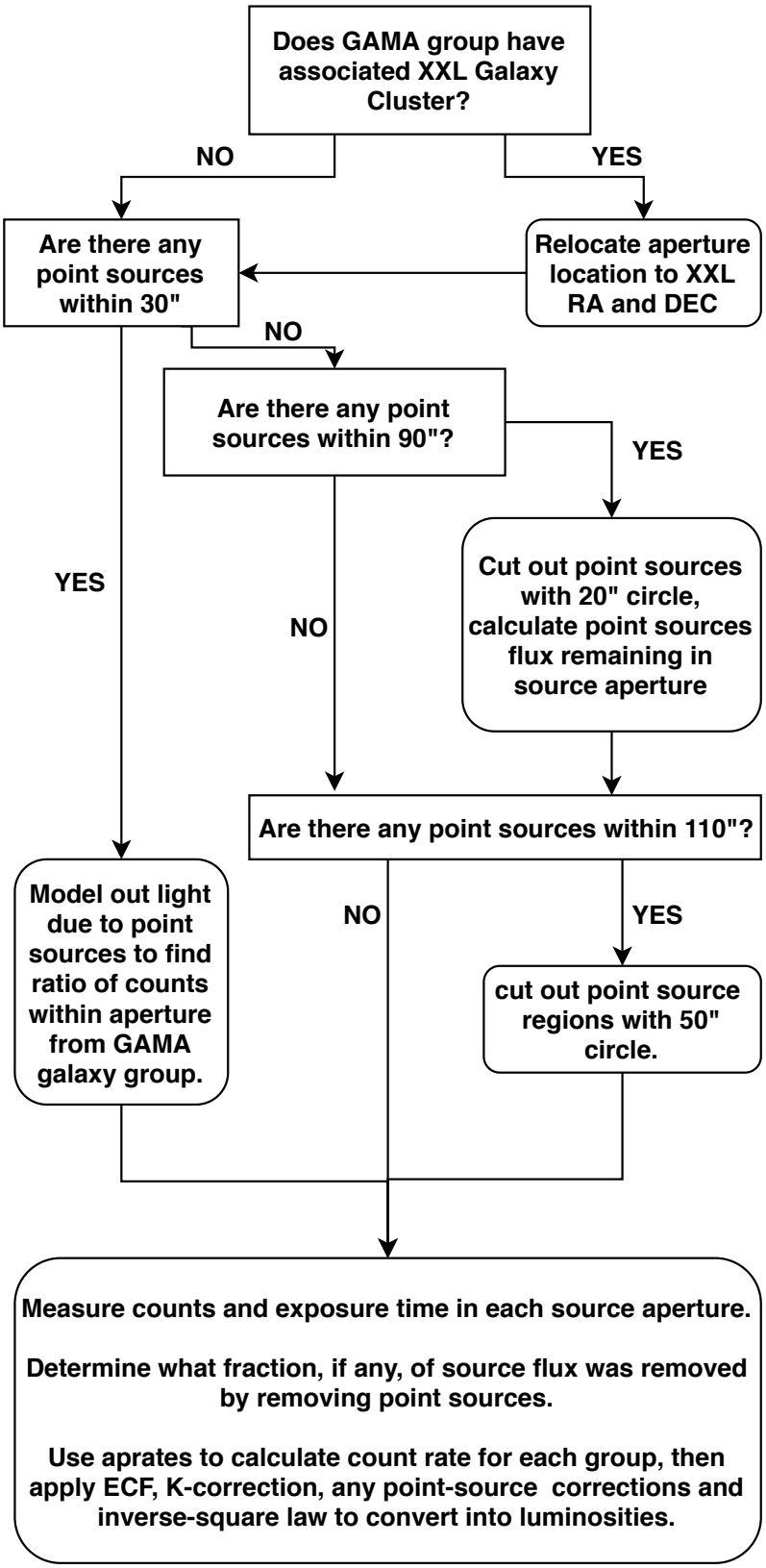

Figure 4: A flow chart showing the procedure used to associate the GAMA groups with XXL sources.

GAMA group 1	Matched GAMA group 2	separation (")	separation (z)	NFoF 1	NFoF 2
400123	400168	116	0.065	6	5
400039	400385	105	0.008	17	5
400060	400305	98	0.100	8	5
400094	400200	86	0.017	7	5
400065	400207	75	0.356	10	7
400096	400208	56	0.034	7	6
400040	400238	52	0.040	12	5

Table 3: GAMA groups located within 120" of each other, along with their separations, and how many members each group has.

this to 53 matches, the four matches removed were individually assessed, and then added back into the sample since they appear to be reasonable matches.

Of the 57 matches, four GAMA groups match to two XXL groups each, resulting in doubles. To account for this the analysis was done for each group individually, and then the luminosities where added and each double was treated as one group. These doubles could be due to early-stage mergers, where the GAMA FoF algorithm has been able to determine that the galaxies are within the same group, but the merging structures are sufficiently distinct to be detected as separate X-ray sources.

2.3.2 AGN and XXL point sources

An issue to contend with is the presence of Active Galactic Nuclei and other X-ray point sources, whose bright X-ray emission may contaminate the group emission. The XXL detection pipeline determines if an X-ray detection is a clear point source, and if so it is labelled bp1. All GAMA groups are matched with the 3XLSS point source catalogue (Chiappetti et al., 2018) for any bp1 classified point sources within 110", and the location, and separation, of each point source noted. A matching radius of 110" was used since the aperture radius used for the forced X-ray photometry of each group was 60" and the radius of the circle used to remove point source emission had a radius of 50". The XXL point source catalogue also contains many unclassified sources, and some of these may be AGN. This was tested by using the ALLWISE AGN catalogue by Assef et al. (2018) and checking how many GAMA groups where matched with an unclassified XXL source which itself matched within 20" to an ALLWISE AGN. Out of 234 groups, only 92 had no point source detected nearby, and the remaining groups need a method to remove the point source contamination.

2.3.3 Matching with other GAMA groups

Each GAMA group is also matched with all the other GAMA groups within 120", with the pairs shown in Table 3. GAMA groups nearby to each other may be due to galaxies not quite being combined into a single group by the GAMA FoF algorithm, else this may represent groups undergoing early-stage mergers, or simple that the galaxy groups are near each other. For this work, each GAMA group is treated separately, and the emission from neighbouring groups masked with a 60" circle.

2.4 X-ray photometry

The process used to determine the X-ray luminosity of each group is based on the method explained by Willis et al. (2018), whereby photon counts and exposure time are determined for a source and

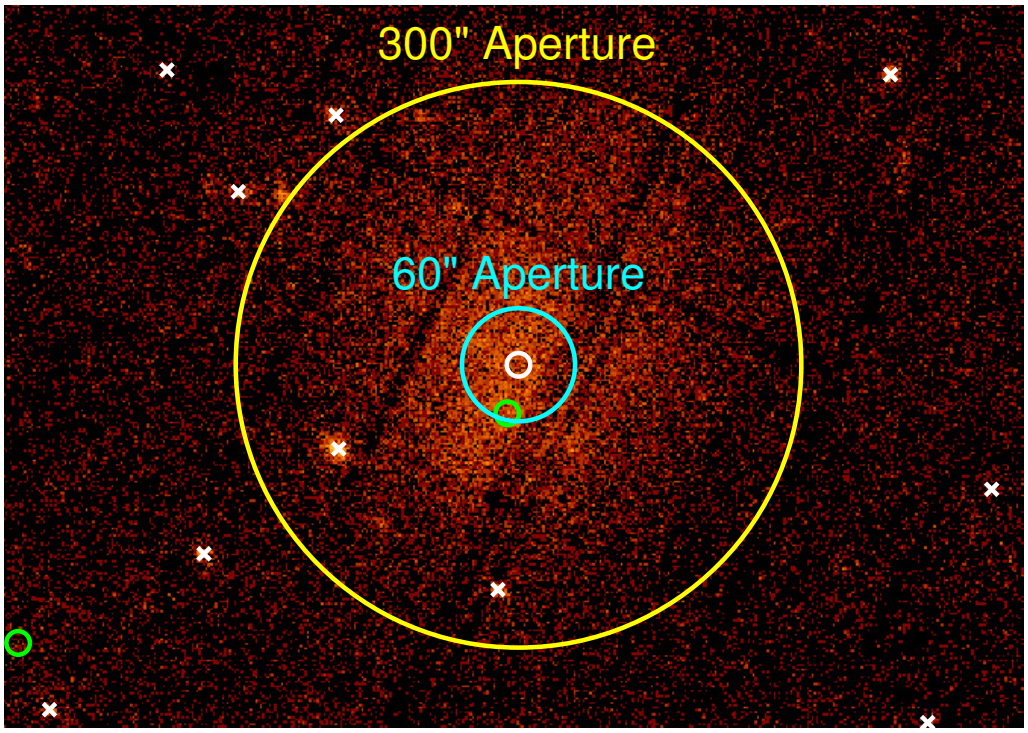

Figure 5: *XMM-Newton* image in the 0.5-2 keV energy band showing the XXL view of GAMA group 400001, with the GAMA coordinates shown by the green circle, the XXL coordinates the white circle, and any XXL point sources shown using white crosses.

background region, and from this the posterior distribution function of the source count rate is determined. Since many of the groups are undetected in the X-ray, forced X-ray photometry is applied at the locations set by GAMA. This method is described below, and returns a luminosity posterior which is sampled in order to deal with the case that there is little or no source signal.

2.4.1 Aperture

A 60" source aperture size is used to extract the source counts, unless the GAMA group matched with an XXL group whose X-ray emission is clearly extended beyond 60", in which case the source aperture is manually extended. This is done for Groups 400001 and 400002, as seen in Figures 5 and 6, however, these are clear outliers in the sample, with all other groups being considerably less bright and less extended.

The aperture used is a circle centred on the GAMA coordinates, unless an XXL group is matched, as discussed in 2.3.1, in which case the XXL coordinates were used. This accounts for the fact that many of the XXL matched groups are slightly off centre to the GAMA coordinates, often only a few arcseconds, and rather than adjusting by eye this is a simpler, and automated, method. The advantage of doing this can be seen in Figures 5 and 6 where the GAMA location, green circle, is slightly off from the X-ray emission centre, the white circle.

Relocating GAMA groups to XXL coordinates could cause a slight bias as these groups would have slightly higher and more accurate count rates than GAMA groups which have not been relocated. Unfortunately, there is likely to be a number of GAMA groups which have just failed to pass the XXL group detection threshold, whose GAMA coordinates would not match the X-ray centroid perfectly. Possibly future work could involve matching GAMA groups with XXL sources

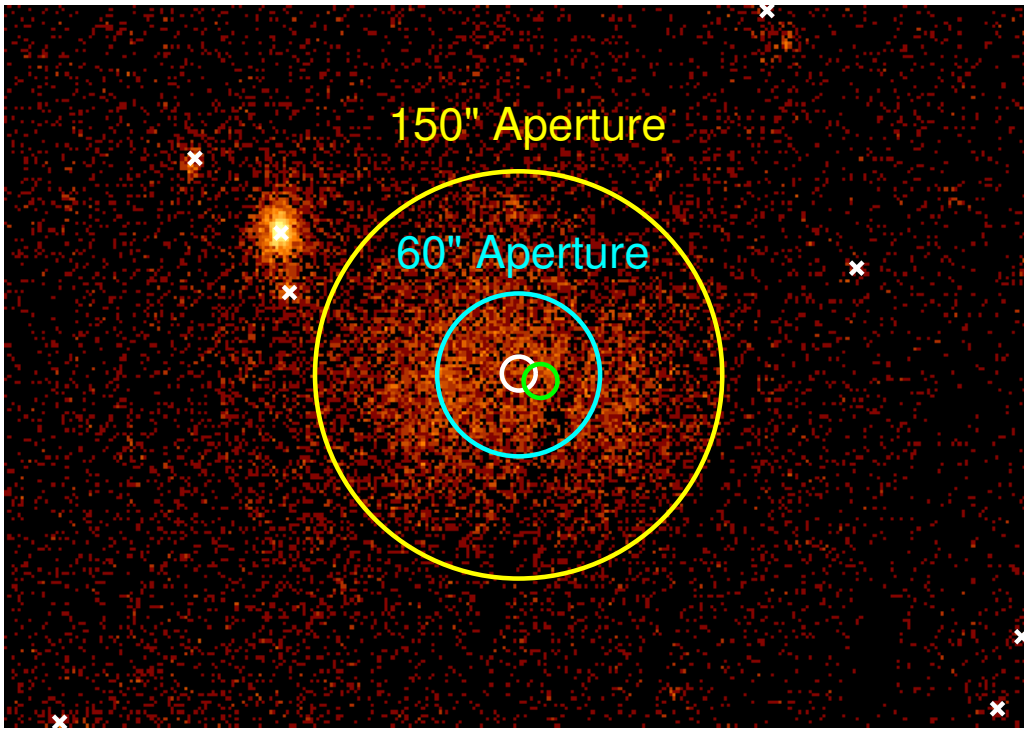

Figure 6: *XMM-Newton* image in the 0.5-2 keV energy band showing the XXL view of GAMA group 400002, with the GAMA coordinates shown by the green circle, the XXL coordinates the white circle, and any XXL point sources shown using white crosses.

with weaker extension likelihood values, manually correcting the group locations or even using a centroid function. However, this could relocate some groups to other non-group X-ray sources, bringing in different issues as the emission may not be group emission.

2.4.2 Background

Since the full XXL North field mosaic is a large file (1.6Gb), splitting it into 16 subregion files, which only include the overlap region, is sensible to reduce computational time and power used to handle and work with the data. The subregion files each have a solid angle of 1.93 deg^2 and as such there is a large amount of overlapping area (14.3 deg^2 total) to ensure that no emission is lost on the edges of a subregion image. Each of the XXL mosaic subregion images were masked so that all XXL point sources, XXL ALLWISE AGN matches and XXL or GAMA galaxy groups are removed. This treatment was done to both the count rate mosaics and the exposure time mosaics, and the remaining counts and exposure times were used to calculate a background count and exposure time for each subregion. The background variation between the subregions is small, with the mean background across the 16 subregions in the GAMA-XXL overlap area being $2.5 \pm 0.1 \times 10^{-6}$ counts/pixel/second.

2.4.3 Core radius

The core radius is an important value since it is used by the β-Model (see Section 1.2.1) to describe the surface brightness profile of the X-ray emission surface brightness profile. This is necessary to account for any counts which may lie outside the source aperture used, and in order to determine how much flux is lost when removing point sources from within the aperture. To account for

flux located outside the source aperture, the surface brightness profile was used to determine the fraction of the flux located within the aperture and then used as a correction to obtain the total flux.

For each GAMA group the dynamical mass (M_{FoF}) is calculated by Robotham et al. (2011), and can be considered equivalent to the virial (or total) mass of the group, which itself is equivalent to M_{200}. M_{200} is known as the mass within a spherical volume of radius R_{200} with a density 200 times the critical density (ρ_{crit}) at that redshift, therefore,

$$R_{200} = \sqrt[3]{\frac{3M_{FoF}}{4\pi 200\rho(z)}}. \tag{15}$$

The relationship between R_{500}, R_{200} and the core radius (R_c) are described by Giles et al. (2016) and Ettori & Balestra (2009) giving:

$$R_C \simeq 0.15R_{500} \simeq 0.15\frac{1}{2}R_{200}. \tag{16}$$

This value of the core radius is, however, only an estimate. The core radius of each group could in theory be calculated for each group, however, the photon counts observed for many groups are so low and diffuse such that they are nearly indistinguishable from the background. The mean value for the core radii calculated is 95 kpc, which matches the average value of 100 kpc found by Koens et al. (2013) for the WARPS sample.

2.5 Removing point source emission

Any point sources which are close enough to contribute to the group emission have to be accounted for, and are treated differently based on how far away from the source they are located, and hence how much they interfere.

2.5.1 Correcting for lost group emission

In any cases where some region of the source aperture is excised to remove a point source, the lost source emission is calculated using a β-model. This is done by using the core radius to create a β-model centred on the group's coordinates applied to the exposure map and smoothed using the PSF, which is described in Section 1.3.1. This is done both with and without the removed regions, and the ratio of flux within the aperture region is calculated. This ratio can then be applied after any corrections are made whereby regions are removed from the source aperture. This is done to correct for the fact that different groups have different core radii based on their size and redshift, and as such the core emission could extend further or not, resulting in the same excluded region having differing effects based on the groups' properties. This also takes into account that the counts near the centre are higher than in the outskirts of the aperture region, and as such when regions closer to the centre are removed, the correction must be larger.

2.5.2 Modelling out point sources within 30"

If any point sources where located within 30" of the GAMA coordinates, then the emission from the group and the point source are too close, and as such cutting out a region would exclude a large fraction of the group emission. An example of this issue is given by GAMA group 400043 and

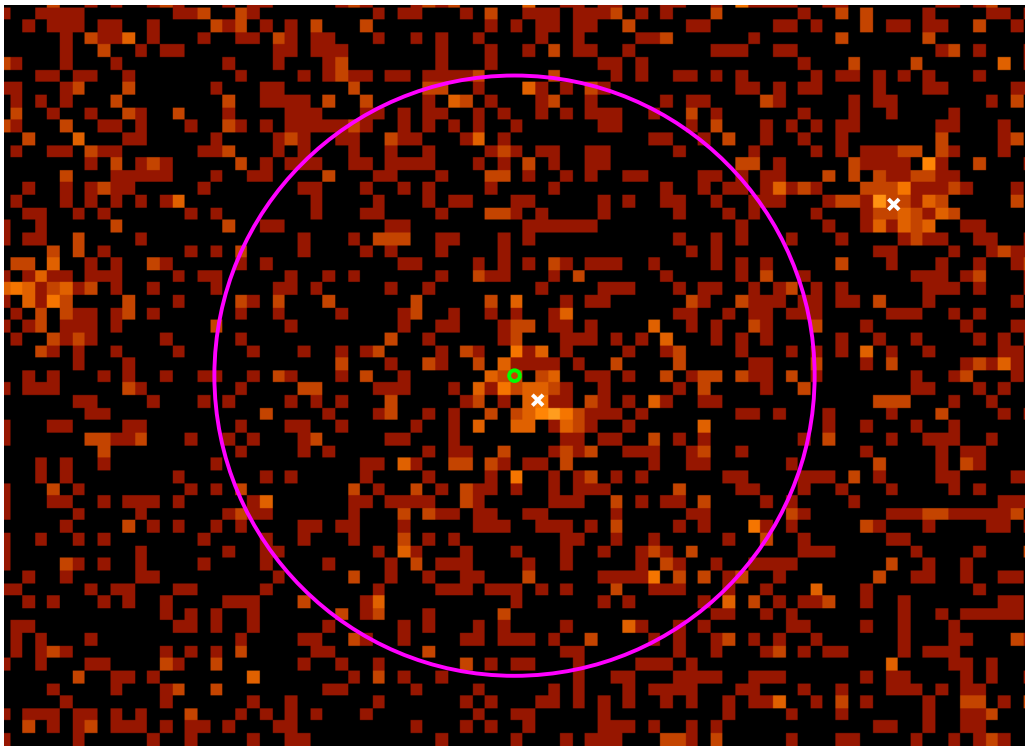

Figure 7: *XMM-Newton* image in the 0.5-2 keV energy band showing the XXL view of GAMA group 400043 with a XXL detected AGN located 5" away from core. With the AGN located so close to the core cutting out a circle would not be feasible without losing most of the group emission. The GAMA group, AGN and 60" source aperture are marked in green, white and magenta respectively.

shown in Figure 7. Here the AGN and group core are only 5" apart, and by eye the emission from the two is indistinguishable. To solve this issue, these groups are manually modelled in Sherpa, the CIAO modelling and fitting application described by Freeman, Doe & Siemiginowska (2001). To do this, a model of the group and any point sources plus a flat background was created. This was convolved with the PSF and multiplied by the exposure map and then compared with the image data. Each group is represented by a 2d beta model, see Section 1.2.1, with the core radius value taken as calculated in Section 2.4.3, and the location taken as the coordinates. Each point source is modelled using a 2d delta function, with the location taken from the XXL coordinates. In some cases there where point sources apparent in the X-ray image data that where not detected by the XXL pipeline which where also included in the model. The model is fit to the data by minimising a Poisson likelihood (Cash) statistic through use of a Nelder-Mead simplex optimisation algorithm. This returns the best fit parameters for each model parameter, which are manually inspected to ensure that they are reasonable.

Once the best fit values are obtained, a ratio can be found between the aperture flux solely due to the group emission and the aperture flux due to all X-ray sources. This means that once the background removed source region count rate value is obtained, multiplying by this value returns the count rate solely due to the galaxy group.

2.5.3 Removing other point sources

Emission from point sources located more than 30" away from the group can be masked out using a circle, however the point source has been spread by the PSF, and so the masked region must

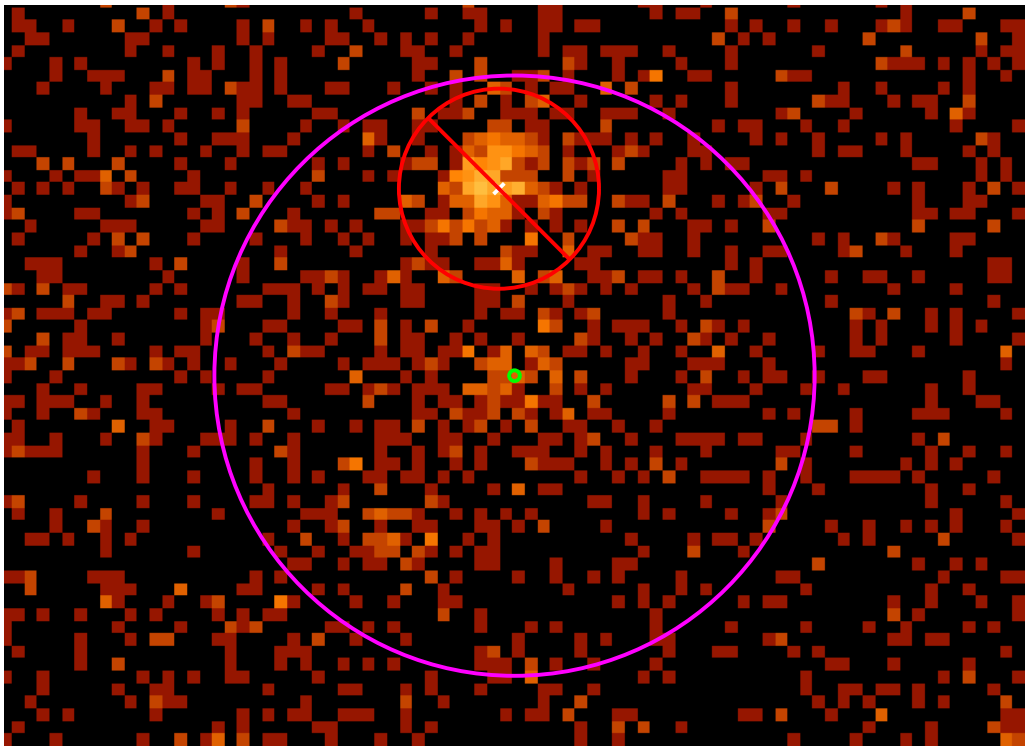

Figure 8: *XMM-Newton* image in the 0.5-2 keV energy band showing the XXL view of GAMA group 400030 with a XXL detected AGN located 40" away from core. The circle used to remove AGN emission is shown in red and the GAMA group, AGN and 60" source aperture are marked in green, white and magenta respectively.

either be large enough to remove most of the spread or the residual flux must be accounted for. If a point source is located between 30" and 90" from the group centre, then a 20" radius circle is cut from the data at the point source coordinates. GAMA group 400043 has an AGN located 40" away from its core, and as seen in Figure 8 the emission from the AGN and group are somewhat separated. The red circle represents the circle cut out to remove the majority of the AGN emission, and the residual emission remaining in the source aperture is calculated. This was done to avoid excluding too much of the group emission, however, this means that only 75% of the flux enclosed within the PSF has been removed, and as such the residual emission from the point source must be accounted for. If a point source is located between 90" and 110" from the group centre, then it is cut out using a 50" circle, which contains 90% of the PSF light, and since it is so far from the group, the maximum possible PSF residual in the aperture region is 1.6%. Therefore the residual emission is essentially negligible and does not need correcting.

The 20" circle used to remove point sources between 30" and 90" from the group contains 75% of the spread from the PSF, and so a non-negligible proportion of the light from the point source is outside the cut region. To account for this, the residual spread from the PSF within the 60" aperture is calculated for different distances between the group centre and the point source centre, and is shown in Figure 9.

Next, a rough point source count rate (A) s calculated from the 20" cut out counts (C) and exposure time (T_C) using

$$A = \frac{C}{T_C} - \frac{m}{T_B} - \frac{n}{T_S}(1-\beta) \tag{17}$$

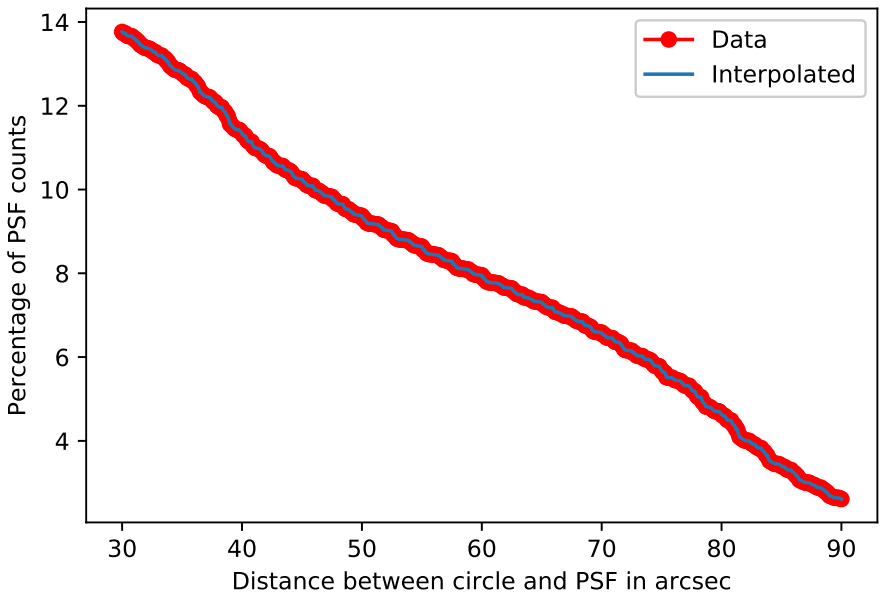

Figure 9: The percentage of PSF counts, excluding inner 20" of PSF, found in a 60" circle as a function of circle distance from PSF centre.

Symbol	Description
n	Source aperture counts
m	Background aperture counts
A_s	Source aperture pixels
A_B	Background aperture pixels
α	PSF fraction in source aperture
β	PSF fraction in background aperture
T_S	Mean exposure time in source aperture
T_B	Mean exposure time in background aperture.

Table 4: Input parameters used by CIAO package aprates (Primini & Kashyap, 2014).

where n and m are the source and background counts, T_S and T_B are the source and background exposure times and β is the fraction of the beta model remaining in the source aperture, described in Section 2.5.1. This point source count rate is then divided by .75 to get the full count rate out to infinity, multiplied by the PSF residual within the 60" aperture region and the background exposure time and then this value is added to the background counts. This new increased background value accounts for the remaining point source counts within the source aperture due to the PSF.

2.5.4 Aprates

The CIAO package aprates is used to calculate the count rates for each group, as described by Primini & Kashyap (2014), using the parameters discussed in Table 4 .

The source count rate, s, and its Gaussian error, σ_s, are calculated using:

$$s = \frac{\frac{A_B T_B}{A_S T_S} n - m}{\frac{A_B T_B}{A_S T_S} \alpha T_S - \beta T_B} \tag{18}$$

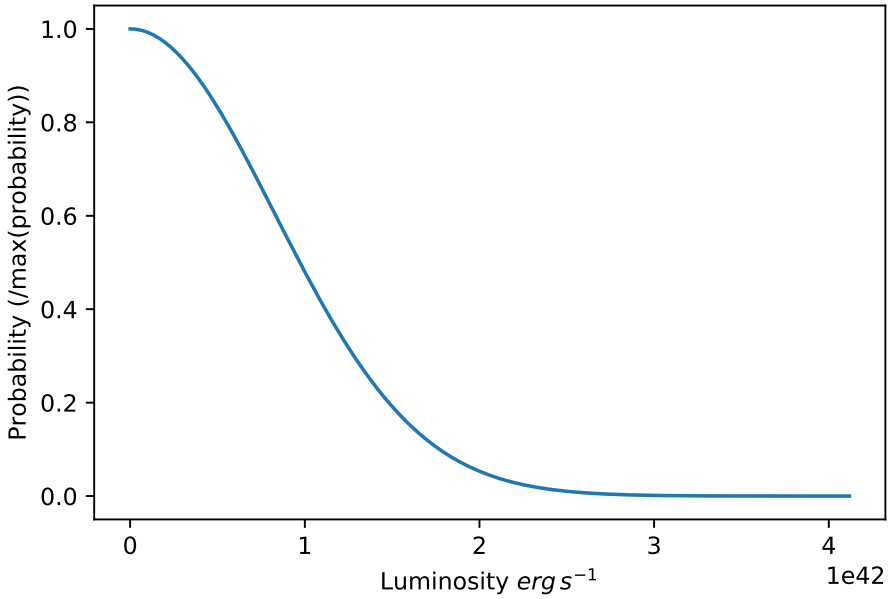

Figure 10: The luminosity posterior for GAMA group 400414 is heavily truncated, with the mode luminosity equal to 0.

and

$$\sigma_s^2 = \frac{\left(\frac{A_B T_B}{A_S T_S}\right)^2 n - m}{\left(\frac{A_B T_B}{A_S T_S}\alpha T_S - \beta T_B\right)^2}. \tag{19}$$

Aprates returns a mode value, with 68% confidence values, for the source count rate, however, in many cases this mode is zero as the background is greater than the source. For these groups aprates truncates the results at zero, and outputs a mode value of zero, an upper confidence value and returns 'INDEF' as the lower confidence value. To work around this issue, aprates returns a probability distribution function (PDF) for each group, some of which have a mode of zero. The zero mode values return a posterior which resembles a truncated Gaussian, such as in Figure 10, therefore, for each group a posterior count rate PDF is saved from aprates, instead of the mode value and confidence limits.

2.6 Luminosities

Having removed and calculated correction values for each group as neccessary, and used aprates to determine a count rate posterior, the count rate must be converted to a luminosity. Converting a count rate to a luminosity is dependant on the properties of the detector used, the flux emitted, the source spectra, the distance to the source and objects located between source and observer. The method used to convert from count rate is discussed here.

2.6.1 Energy conversion factor

An energy conversion factor (ECF) is used to convert from count rate to flux. The ECF depends on the instrument response files, the shape of the source spectrum and absorption which occurred

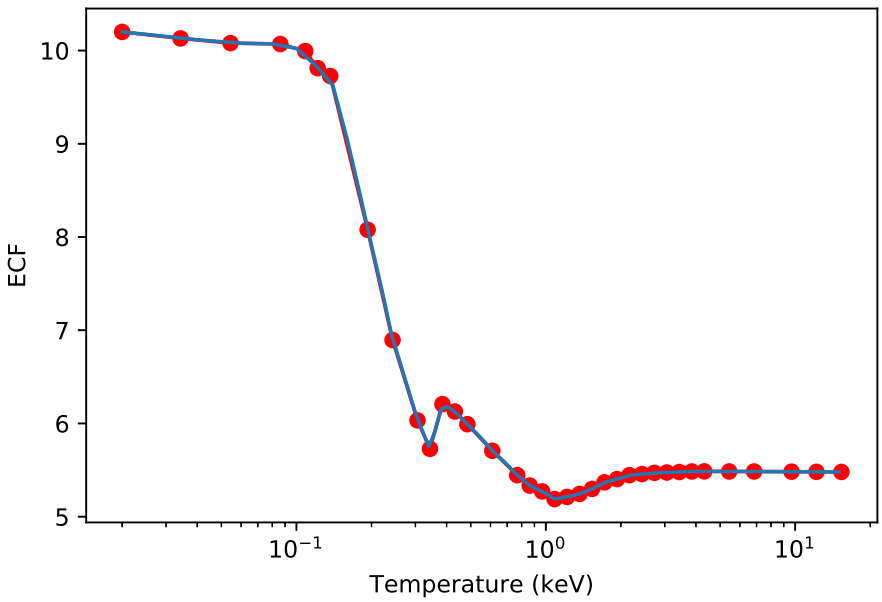

Figure 11: Plot showing how the energy conversion factor, stated in units of $\times 10^{-12}$ erg s^{-1} cm^{-2} for a count rate of one count s^{-1}, varies as a function of group temperature. Each point is taken from webPIMMS using the APEC model with abundance set to 0.4 solar abundance, nH to 2.51 $\times 10^{20}$ cm^{-2} and redshift 0.

between the source and detection. The ECF was calculated for a range of source temperatures using the online tool, WebPIMMS. The source model used is APEC, described by Smith et al. (2001), with the galactic nH value set to 2.51×10^{20} cm^{-2}, the abundance to 0.4 solar abundance and the redshift to 0. The resulting ECF values, as a function of temperature, are shown in Figure 11 with the blue line showing an interpolation used to be able to determine the ECF for any given temperature. The high values for the ECF at low temperatures exist due to a combination of many factors, including that nH absorbs a greater proportion of, and that the CCD is less responsive to, low energy photons. The troughs seen at $\sim$ 0.15, $\sim$ 0.35 and $\sim$ 1 keV are where the outer k-shell edges of carbon, nitrogen and oxygen have respectively absorbed photons. For each group the temperature was estimated by using the M-T relation by Lieu et al. (2016) on the mass values calculated by GAMA (Robotham et al., 2011).

2.6.2 K-correction

The XXL mosaic count-rates were measured in the 0.5-2.0 keV band, however, due to the expansion of the Universe this will correspond to a different band in the rest frame of the group. To ensure the luminosity is from a consistent band, the flux from each group is converted to the 0.5-2.0 keV rest-frame band by multiplying the measured flux by some number K, called the K-correction.

Since the K-correction depends on the spectral model of the group, the APEC model is used again, however, since nH is accounted for by the ECF, its absorption effects are ignored here, and the abundance set to 0.3 solar abundances. The temperature is again calculated using the M-T relation by Lieu et al. (2016), and the redshift taken from the GAMA catalogue. The K-correction is calculated for each group using Sherpa, and then stored to convert the flux into the 0.5-2.0 keV

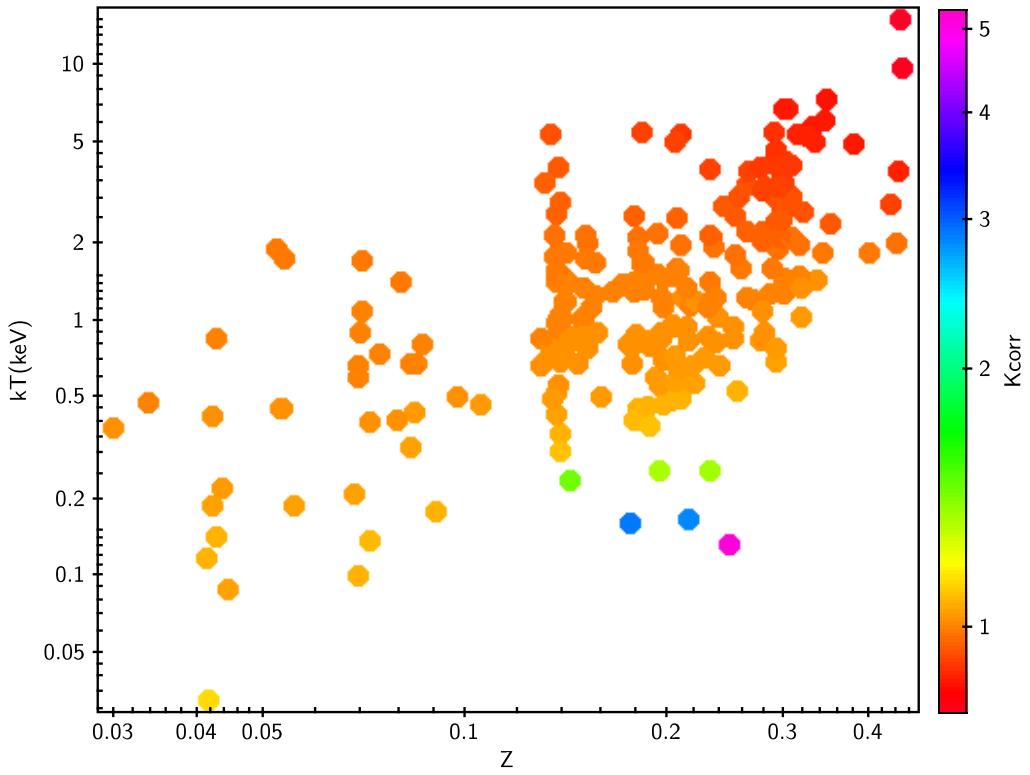

Figure 12: Colour map showing how the K-correction values for each group depend on the group's redshift and temperature. Clearly higher redshift and low temperature groups have a very high K-correction. All 234 GAMA groups are plotted here.

band. The mean K-correction value for the groups is 1.04, with a standard deviation of 0.33.

There are three major outliers, groups 169, 459 and 414, whose K-correction values are 5.275, 2.913 and 2.853 respectively, however, these values can be explained by looking at Figure 12. Low temperature spectra have a sharp change in shape at certain energies, and this effects the K-correction value at higher redshift as the energy band is shifted over this sharp change. This may mean that any uncertainty on the temperature could give a large change in the K-correction in these, and similar, groups. Future work will test the impact of this by including the temperature uncertainty in the calculation of the K-correction.

2.6.3 Converting count rate to luminosity

The count rate posteriors are first corrected for contaminating point source emission by multiplying them by the ratio calculated in Section 2.5.2, then correcting for the flux lost due to excluded regions as calculated in Section 2.5.1. The next step is to analytically calculate what ratio of the total β-model emission is enclosed within the aperture using the core radius and Equation 12 as described in Section 1.2.1, and multiply each count rate posterior in order to obtain the count rate posterior for each group's emission out to infinity. These total count rate posteriors are then multiplied by the ECF which returns the flux posterior, and using the inverse square law and the luminosity distance this is converted to the luminosity posterior in the observers frame, and so the K-correction is applied such that the final luminosity posteriors are in the 0.5-2.0 keV rest-frame energy band for each group.

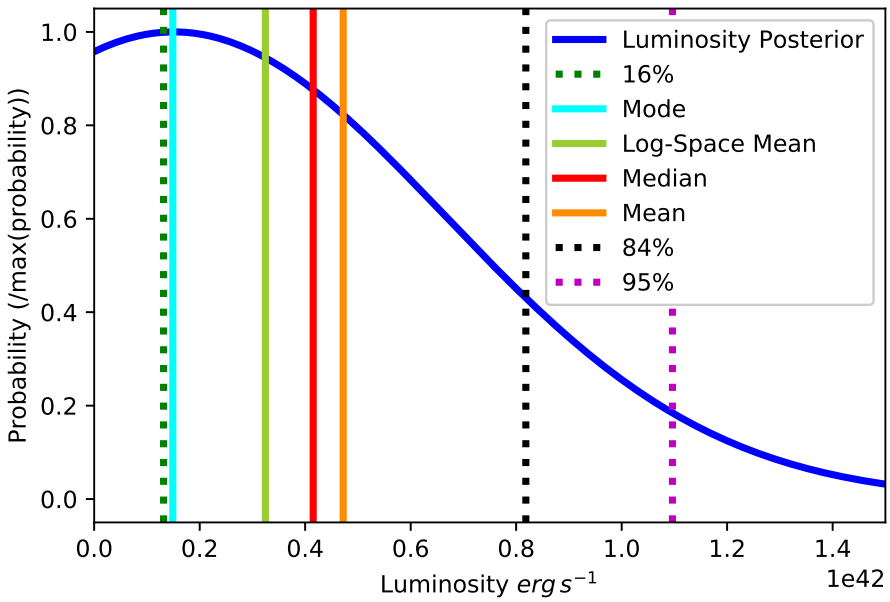

Figure 13: The luminosity posterior for GAMA group 400200 with possible representations of the luminosity of the group marked.

2.6.4 Sampling the luminosity posteriors

Many of the groups returned truncated luminosity posteriors, such as that of GAMA group 400200 shown in Figure 13. In order to have a representative value for the luminosity of each group, some method is needed to represent the luminosity posterior in a numerical form. For the non, or only lightly truncated posteriors the mean, median and mode values are the same, however, when the posterior is truncated these values vary greatly. As is seen in Figure 13, the mode of the group is considerably less than the median for a truncated posterior. Since the luminosity posterior represents a probability distribution of the luminosity of the group, the best representation is the median with errors given by the 16% and 84% values. While the mode is the most likely luminosity of the group, it is not as good a representation of the possible luminosities of the group. The 95% represents a realistic maximum for the group luminosity, and depending on the group features being analysed could prove useful.

For the sake of the XLF, the luminosity does not in fact have to be one value, and as such the luminosity posterior is sampled many times. This allows a good representation of the luminosity of each group as the luminosity posterior ends up being sampled 1,000 times, with each realisation of the possible XLF being found from a different realisation of each groups posterior.

3 The X-ray luminosity function

3.1 Method of calculation

For each group the V_{max} and luminosity posterior has now been calculated, and so the XLF can be fit as described below.

3.1.1 Luminosity bins

As discussed in Section 2.6.4, there are many definitions of the luminosity, and each leads to varying results for the low-luminosity bins. The method used to define the luminosity bins for the XLF is to set each bin manually, so that each bin should have between 10 and 20 groups for any given realisation of each group's luminosity. This allows for the luminosity posteriors to be sampled many times, and for each sample the number density in each bin is calculated with the same bin boundaries used. The median luminosity of all the groups within the bin is then used as the luminosity value for the bin, such that if a disproportionate amount of groups within a luminosity bin are skewed, the median luminosity used represents this.

The number density of each luminosity bin is then calculated by summing over N groups in each bin of width ΔL using

$$n = \frac{1}{\Delta L} \sum_{i}^{N} \frac{1}{V_{max,i}} \tag{20}$$

where $V_{max,i}$ is the maximum comoving volume at which the ith group can be observed, as described in Section 2.1. This is then repeated 1,000 times until each bin has 1,000 realisations for its number density, from which the mean value (n) and standard deviation (n_{err}) are calculated based on a Gaussian distribution, along with the mean number of groups (N) in each bin. The error on the number density (σ') is then a combination of the standard deviation and the standard error given by

$$\sigma' = \sqrt{n_{err}^2 + \left(\frac{n}{\sqrt{N}}\right)^2}. \tag{21}$$

3.1.2 Fitting a Schechter function

The XLF is fitted by a Schechter function (Equation 14), with an MCMC algorithm (see Appendix B) used to determine the best fit parameters. The likelihood function finds the probability of observing $\log_{10}(n)$ (Equation 20) in each luminosity bin from a log-normal with the mean being $\log_{10}(n_{model})$ found using a Schechter function, and $\sigma = \sigma' \frac{n_{model}}{n}$.

Since the highest luminosity group in the sample has a lower luminosity than the L^* value found by REFLEX II, it is not viable to set L^* as a free parameter since the data would be unable to constrain its value reasonably, even with a prior, and as such it is locked at the REFLEX II value. This means MCMC is run through $\log_{10}(n^*)$ and α space in order to find the best fits for these parameters, with the MCMC chains starting with $\log_{10}(n^*)$ and α values based of REFLEX II with a random variation of 10%. Non-informative priors are used, such that the posterior simply represents the likelihood function.

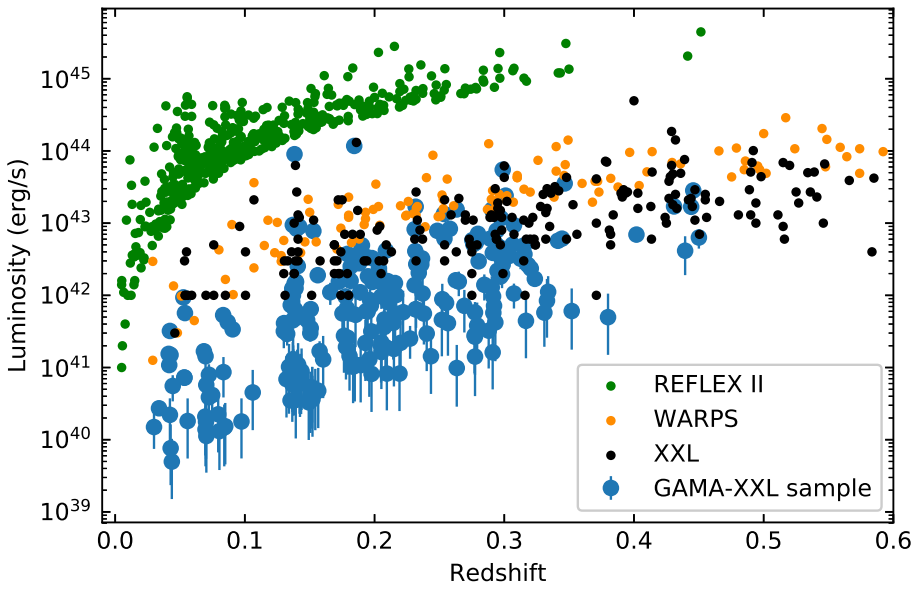

Figure 14: Comparisons between the X-ray luminosity and redshift distribution of the median X-ray luminosity for each group in the GAMA-XXL sample of 234 groups with the values found by Böhringer et al. (2004); Horner et al. (2008); Adami et al. (2018) for 802, 124 and 365 galaxy groups respectively. The redshift range is limited to a maximum of 0.6, however the WARPS and XXL catalogues extend up to redshifts of 0.92 and 1.99 respectively.

3.2 Results

3.2.1 Luminosities

The luminosity posteriors obtained for each group are represented using the Mode, 95%, Median, 16% and 84% by Table A1, and are compared in redshift space to the luminosities of the groups in the WARPS, REFLEX II and XXL catalogues in Figure 14. It is clear that the luminosities observed are of an order of magnitude fainter than the X-ray selected samples up to redshifts of 0.4, allowing for a greater constraint on the faint end of the XLF in the local Universe.

3.2.2 The XLF

The XLF shown in Figure 15 is determined as described in Section 3.1. The best fit Schechter function parameters agree well with the results determined by Koens et al. (2013) when using the WARPS data. The method used to determine the XLF shown in Figure 15 has the added caveat that the final luminosity bin, including any groups with a luminosity greater than $10^{43.5}$ erg s^{-1}, is excluded from the calculations. Figure 16 shows the mean number of groups per luminosity bin, and shows that the excluded high luminosity bin contains on average only four groups which are spread over a large luminosity range. The high luminosity groups are excluded due to the small number statistics involved and the large spread of luminosity and number density. Since this work concentrates on the low luminosity region of the XLF, the exclusion of the high luminosity groups is of little consequence to the results. The mean number of groups per bin was used since the number changes with each realisation of each groups luminosity. For transparency, Figure 17

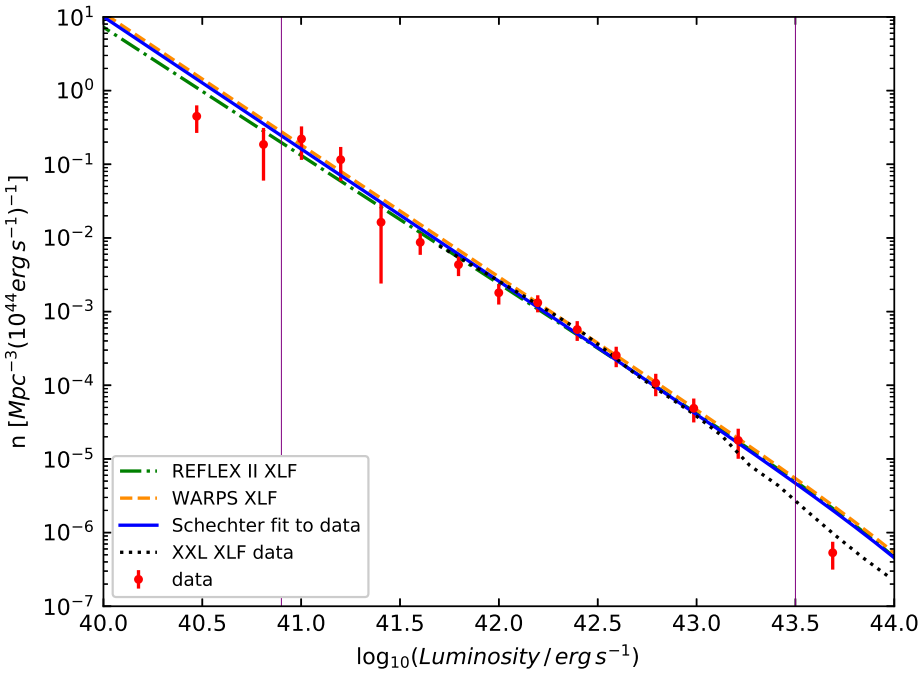

Figure 15: XLF of the optically selected GAMA-XXL galaxy group sample. The fits were performed between the two vertical lines at $10^{40.9}$ erg s^{-1} and $10^{43.5}$ erg s^{-1} which represent the values where incompleteness becomes an issue. Of the 234 groups studied, an average of 180 have luminosities in the luminosity range fitted.

Survey	Number	L_{min}	n^*	α
GAMA-XXL	180	0.0008	3.24 ± 0.10	1.80 ± 0.09
GAMA-XXL inc. high L	186	0.0008	3.09 ± 0.10	1.82 ± 0.06
WARPS	124	0.01	3.68 ± 0.87	1.79 ± 0.04
REFLEX II	910	0.0019	5	1.74 ± 0.05

Table 5: The best fitting XLF parameters found using the GAMA-XXL overlap sample and compared to results by Koens et al. (2013) and Böhringer, Chon & Collins (2014). n^* is quoted in units of 10^{-7} Mpc^{-3} while L_{min} and L^* in units of 10^{44} erg s^{-1}

shows how the Schechter fit changes when this group is included.

Table 5 compares the Schechter function best fit parameters for the GAMA-XXL overlap region sample used with the values found by Koens et al. (2013) and Böhringer, Chon & Collins (2014). The best fit parameters found when including the high luminosity bin as in Figure 17 are included, however, these results are only shown for completeness and unless specified are not discussed again. The values are in better agreement with WARPS than REFLEX II despite the latter including lower luminosities.

The Schechter function parameter posteriors are shown in Figure 18. n^* was sampled in logged parameter space, and so the resulting posterior is a log-normal in non log space, and as such all posteriors are summarised using the median and 16th and 84th percentiles.

These values are summarised and compared with the values found by Koens et al. (2013) and Böhringer, Chon & Collins (2014) in Table 5.

Figure 19 shows the difference between the observed and expected number densities from the

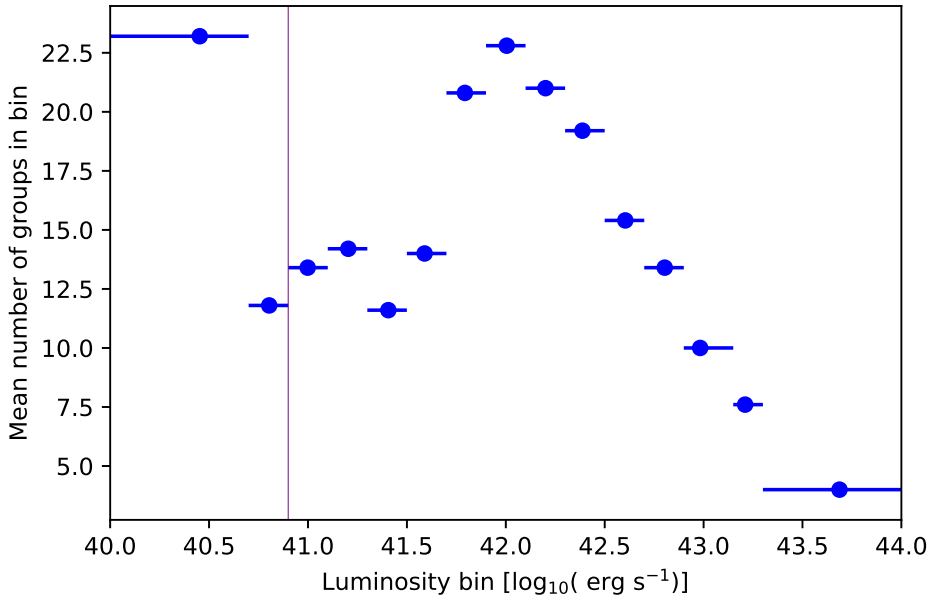

Figure 16: The mean number of groups per luminosity bin for the XLF as seen in Figures 15 and 17. The luminosity value used is the mean luminosity of the groups found within each bin, with the errors showing the bin width.

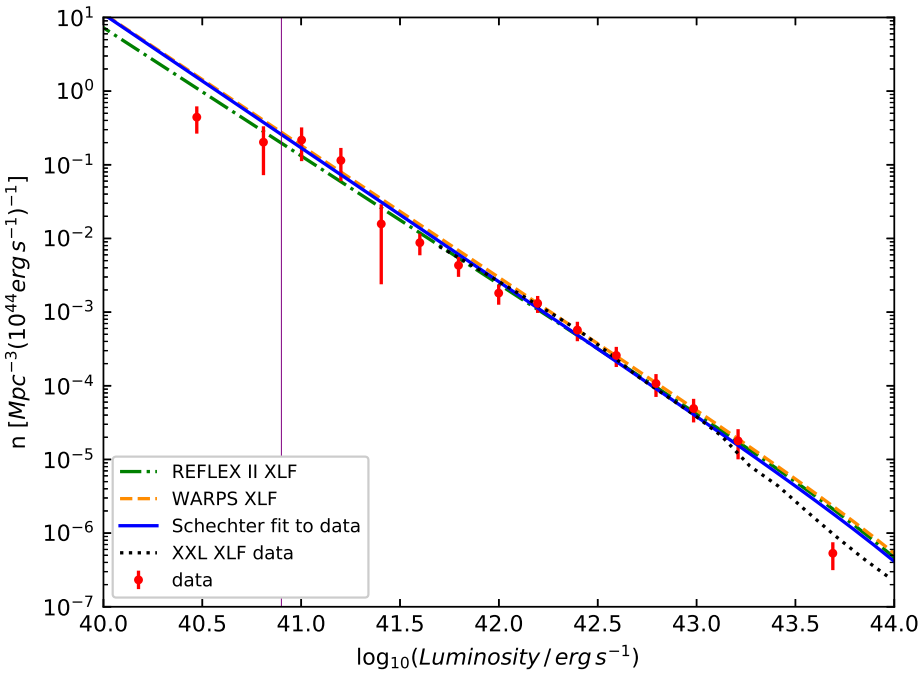

Figure 17: The XLF as seen in Figure 15 with the final luminosity bin included in the calculation of the Schechter best fit parameters. Of the 234 groups studied, an average of 186 have luminosities in the luminosity range fitted.

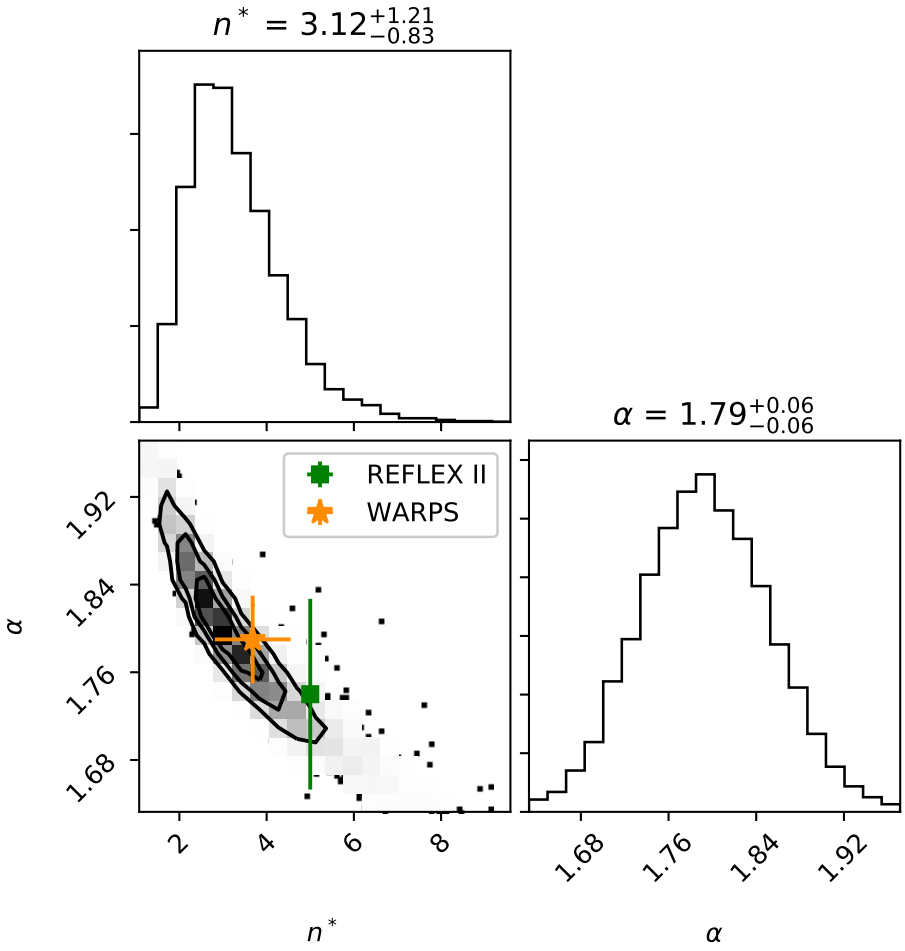

Figure 18: The posterior chains of the best fit parameters for the Schechter function fit shown in Figure 15 for an average of 180 of the 234 groups which lay in the luminosity range which was fitted. These were found using an MCMC algorithm and summarised using histograms and a density plot.The contours show the 1, 2 and 3 σ levels which correspond to the 39%, 86% and 99% confidence values. n^* is given in units of 10^{-7} Mpc^{-3}. The WARPS and REFLEX II parameter values and errors are shown.

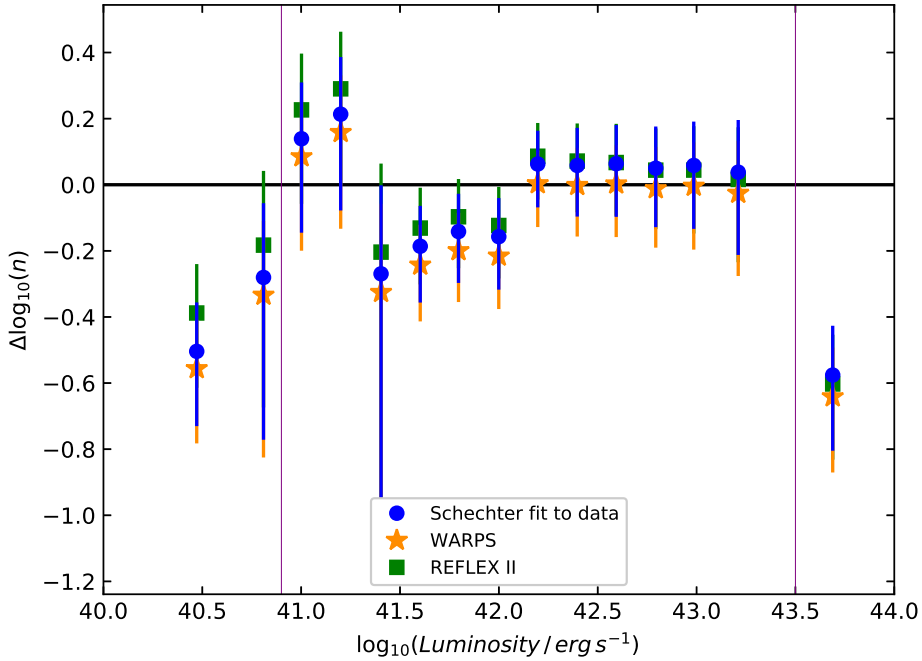

Figure 19: The difference between the observed log of the number density from the XXL-GAMA data and the log of the expected number density from three different reference XLFs.

Schechter functions found using the parameters from Table 5. The lack of groups in the luminosity range $10^{41.4}$ to $10^{42.2}$ erg s^{-1} is clear to see.

To first order, Figure 15 implies that the Schechter function is a reasonable description of the XLF down to luminosities of roughly 10^{41} erg s^{-1}. This extends to lower luminosities than the work by Koens et al. (2013) and Böhringer, Chon & Collins (2014), which only fit to luminosities above 10^{42} and $10^{41.5}$ erg s^{-1} respectively.

At luminosities below $10^{40.9}$ there appears to be a deficit in the number density of groups, however, as discussed in Section 4 the GAMA-XXL sample suffers from incompleteness and may possibly be overestimating the luminosities.

4 Discussion

The results were found using forced X-ray photometry to measure the luminosities for the optically selected group, and as such we were able to explore lower X-ray luminosities than X-ray selected samples. The initial results indicate that the Schechter function remains a good representation of the XLF down to luminosities of 10^{41} erg s^{-1}, however, the issue of incompleteness must be explored further before this is confirmed. The various systematic uncertainties of the luminosities and their effects on the results are discussed. Alongside this a comparison is made to noted deviations from the Schechter function by the REFLEX II survey, and possible explanations for a deficit in low luminosity groups explored.

4.1 Systematic uncertainties on the luminosities

Since the group sample is optically selected, there are many uncertainties on the X-ray luminosity due to location, low-count rates and the methods used. The luminosities of groups without XXL group detections are determined based on the coordinates given by GAMA which may not exactly match the centre of X-ray emission resulting in the potential loss of counts and underestimation of some groups luminosities. To check the sensitivity of the results to the source aperture locations, the aperture could be relocated such that the BCG is used as the centre. Another check would be to apply a centroid function to the aperture locations in order to make minor adjustments to the location based on the X-ray emission shape in the aperture. Using the BCG instead of the iterCEN galaxy will have minimal effect since for 86% of the groups these are the same galaxy, while using a centroid function will lead to an increase in the luminosity of most groups. While this increase in the luminosity will partially be due to the aperture being better centred on the X-ray emission, it will also be influenced by other X-ray sources since the centroid function will always look to get the most counts as close to the centre as possible. The sensitivity of the results to the aperture location will be tested by repeating the analysis with all apertures centred on the iterative centre regardless of whether there is an XXL detection. To determine the reliability of the luminosity results obtained, they are compared to known values from Adami et al. (2018) and Crossett et al., (in prep).

4.1.1 Comparing with XXL luminosities

When comparing the luminosities obtained with the XXL values for matched groups a clear bias is noticed, with XXL having slightly higher luminosities. This can be seen both when matching with the median luminosities in Figure 20. This could be corrected for by finding the offset and adjusting all luminosities accordingly, however, this offset is difficult to compute for the lower luminosities and extrapolating beyond the lowest XXL luminosity would greatly effect the values and introduce a large scatter. As seen in Figure 20 the offset is related to the luminosity, with the best fit correction as high as 591% at a luminosity of 10^{41} erg s^{-1}. Due to the large uncertainties involved, this correction was not applied however future work could determine a more descriptive correction for the offset in XXL luminosity values with the errors included, and this correction could be folded into the luminosity derivation along with the uncertainties involved.

The XXL luminosities where derived using a detailed X-ray background analysis, described in Pacaud et al. (2016). This included the source temperature being determined within 300 kpc and the background was modelled using an annulus encompassing the same off-axis range for each

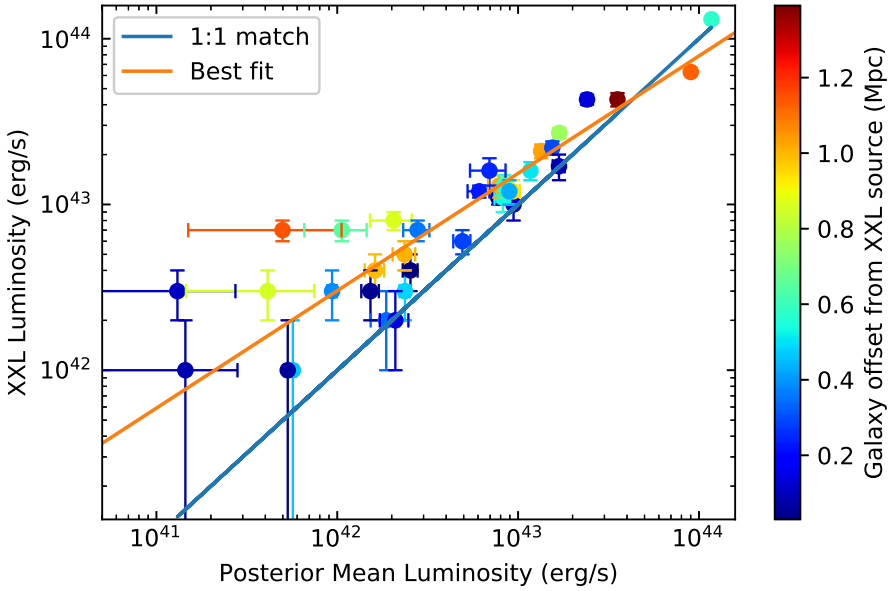

Figure 20: Comparison between the median of each luminosity posterior with the values and errors given by XXL (Adami et al., 2018) for the 53 GAMA groups which had XXL matches. The median luminosity errors are the 16% and 84% values. The best fit is estimated to be is a linear fit with a slope of 0.71 and a normalisation of 12.74. The colour-bar represents the distance between the XXL and GAMA locations.

instrument, or if the source was central then a surrounding annulus was used. This extra level of analysis means that the XXL luminosities are more reliable, as expected, and this level of analysis with the GAMA-XXL sample since the quality of data is far to low for most of the groups.

The result of this is that there may be a systematic underestimation of the X-ray luminosities, as determined when compared to the values calculated by Adami et al. (2018) as seen in Figure 20. This difference increases for the lower luminosity groups, however, the errors given for the XXL values become very large, and as such determining the effect of the difference in luminosities is non-trivial.

4.1.2 Comparing with Crossett et al. (in prep) luminosities

Values obtained from Crossett et al. (in prep) on the same GAMA groups using the same XXL-field data are also compared to our values, as shown in Figure 21. The Crossett et al. (in prep) values are obtained by taking the posterior mode value, and where that is not possible, the 95% upper limit is used. Crossett et al. (in prep) used an aperture size of 300kpc, which is then scaled based on each groups redshift. This method is done since Crossett et al. (in prep) initially explored the higher redshift groups, however, when exploring lower redshift groups a 300kpc aperture is very large and results in a large amount of noise and contamination.

By exploring the difference in luminosities as a function of redshift, NFoF and core radius, no trends where observed. When comparing Crossett et al. (in prep) luminosities to the XXL luminosities the same trends are observed as in Section 4.1.1. Crossett et al. (in prep) goes further to estimate the difference to the XXL luminosity relative to the offset between the GAMA and

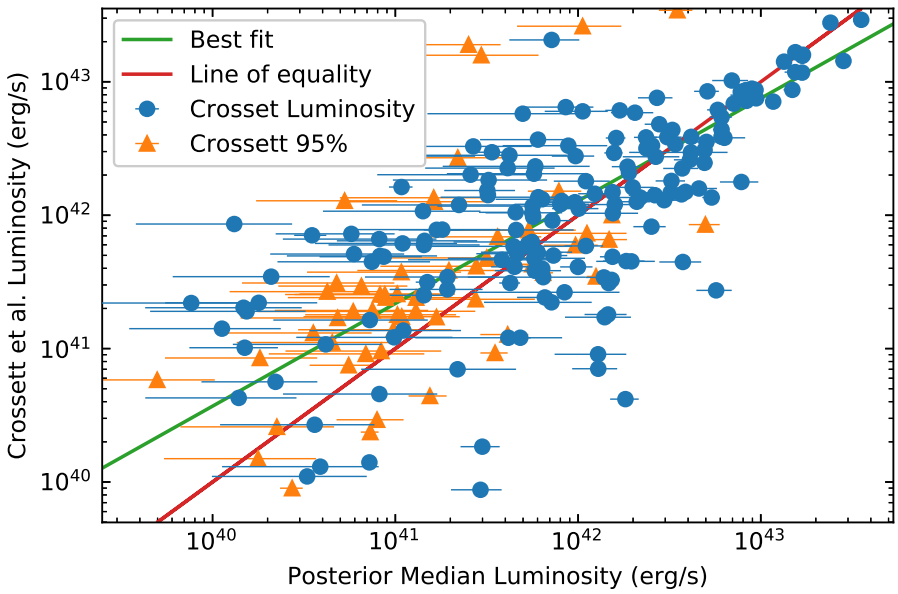

Figure 21: Comparison between the median each group luminosity with the values given by Crossett et al., (in prep). The errors are given by the 16% and 84% values. The best fit is estimated to be a linear fit with a slope of 0.77 and a normalisation of 9.80. The matching done here was for the 228 GAMA groups which where both analysed by Crossett et al., (in prep) and in this work.

XXL locations, and determines that the clear outliers visible in Figure 20 have a larger offset of the order of 1 Mpc instead of the typical offset being in the range 0-400 kpc.

4.2 Number density and luminosity errors

The analysis method used means that the errors on the number densities and luminosity of the bins in the XLF are not independent. Since the luminosities are obtained by randomly sampling each group's posterior, the values vary and as such for any given realisation, a group's luminosity will differ. This results in groups occasionally switching bins, hence the number of groups in each bin differs for each realisation. Therefore, the mean luminosity of each bin and its number density both change when a group leaves or enters said bin. The fewer groups in a bin, the larger the effect of this switching and so the error on the number density incorporates this by being a combination of the number density standard deviation and the mean number of groups in the bin.

The XLF is completely independent of binning, and as such the binning method used should not influence the results. To test this the XLF was calculated with a different method of binning whereby for each realisation of the luminosity space the sample was binned such that each luminosity bin contained 10 groups. This was then fit to find the best fit parameters, and then repeated 1,000 times such that the luminosity space was well sampled, and the resulting XLF shown in Figure 22. The n^* and α values obtained are $3.65 \pm^{6.78}_{2.44} \times 10^{-7}$ Mpc^{-3} and 1.73 ± 0.18 respectively, which is in good agreement with the values shown in Table 5.

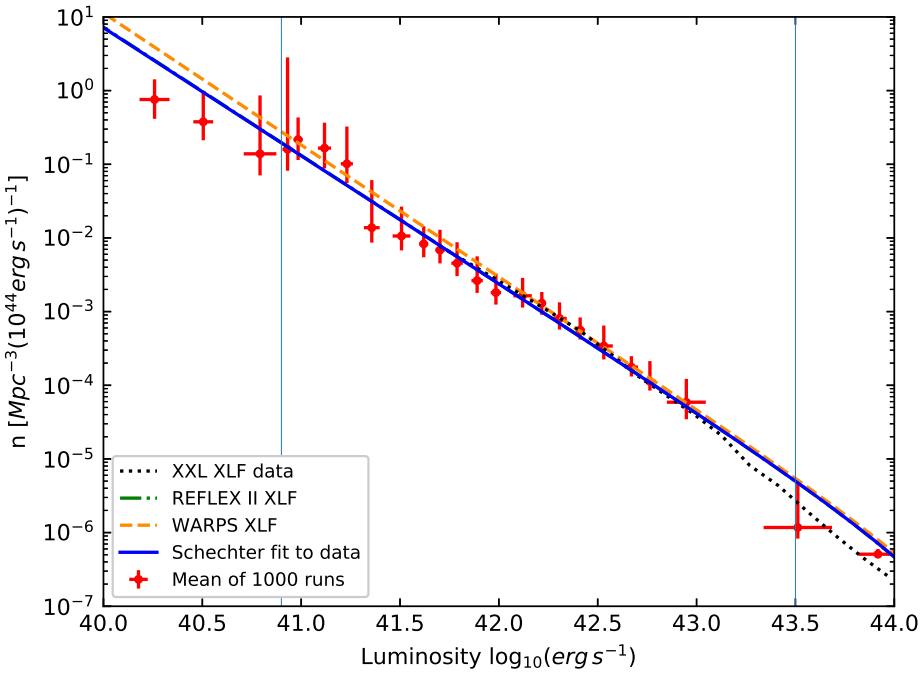

Figure 22: The XLF fit as in Figure 15 with the added caveat that only 10 groups are located in each bin.

4.3 Limitations of the fitting method

Standard procedure when discussing the XLF is to calculate the number of observed and expected groups per luminosity bin. For X-ray selected samples, this is straightforward since the V_{max} is directly related to the luminosity, since the selection function is X-ray based. For the GAMA-XXL sample used here, this is not the case since the V_{max} value is found optically, and so is dependent on the optical luminosity. Furthermore, it is dependent on the optical luminosity of the fifth brightest galaxy in each group and so also dependent on the group's richness alongside its optical luminosity. Future work will change the method used to fit the XLF, as discussed in Section 5.1, such that the expected number in each luminosity bin can be obtained and so the expected versus observed number of groups in each bin will be calculated.

4.4 Accounting for incompleteness

The data points in Figure 15 clearly drop below the best-fitting Schechter function model at very low luminosities, and this is most likely due to incompleteness in the sample, as discussed in Section 2.2. The selection function for a galaxy group to be selected for the sample is that it must have five detected members in the GAMA survey. However, two galaxy groups with the same X-ray luminosity could be treated differently if they have more than or fewer than five galaxies above the GAMA threshold. This issue results in the number of low-luminosity groups being underestimated. A first order correction for this is to remove bins from the fit below the X-ray luminosity at which the optical incompleteness becomes significant.

In order to estimate the region with incompleteness issues, the expected luminosity as a function

of number of member galaxies is estimated. A fit is found between mean group luminosity and richness in log-space, and extrapolated to estimate the mean luminosity for groups with four members, as seen in Figure 23. The observed richness of any group is partially dependant on the groups redshift, and to try and negate for clear outliers a richness value was only used if three or more groups had that richness. Assuming that the distribution of groups with five members is similar to that for groups with four, the standard deviation of the luminosities of groups with five members is found, and used as the standard deviation for the groups with four members. This results in the mean luminosity and standard deviation of groups with four member galaxies to be estimated as $10^{40.9\pm0.6}$ erg s^{-1}. The results discussed in Section 3.2 have used this result as a first order correction, with the data only fit for luminosities greater than $10^{40.9}$ erg s^{-1}.

In order to better account for this incompleteness, the estimated number densities and luminosities of the groups with four members were included to the GAMA-XXL sample, and the change to the XLF found. The GAMA-XXL overlap region contains 161 GAMA detected groups with four members, and their luminosities were estimated by sampling the X-ray luminosity from a Gaussian distribution with mean and standard deviation $10^{40.9\pm0.6}$ erg s^{-1}. These groups where then binned as in Section 3.1.1, and to calculate the increase in the number density for each bin, the mean V_{max} for each bin from the data used in Section 3.2.2 is used as V_{max} for each group in that bin. This new number density is then calculated for each luminosity bin, but again only fitted above $10^{40.9}$ erg s^{-1}. The reason for not correcting below this is that the incompleteness due to groups with even fewer members is also introduced. After calculating the new number densities in each bin, the XLF is fitted as in Section 3.1 and the results shown in Figure 24.

This approximate correction for incompleteness has some limitations. Firstly, the richness calculated for a given group is based on the number of galaxies detected by GAMA. Since higher X-ray luminosity groups are rarer, they are likely to be further away and as such are more likely to have a higher richness than the number detected compared to nearer and less luminous groups. This means that the richness of the high luminosity groups is more likely to be underestimated than the richness of low luminosity groups, resulting in the slope shown in Figure 23 steepening. However, due to the completeness of the GAMA sample in terms of detecting galaxies being 95%, and in terms of matching all galaxies to their respective groups being 77% (Robotham et al., 2011), the resulting increase in steepness of the slope should only increase the mean luminosity of groups with four members by a maximum of 27%. Secondly, the method used to estimate V_{max} for each luminosity bin is introducing an X-ray selection bias since the initial V_{max} values introduced are independent of X-ray luminosity. The V_{max} values will also be underestimated as the selection function to calculate V_{max} is the volume at which the fifth brightest galaxy in each group can be detected. Since the groups with only four members do not match this selection function a new selection function is needed to find a new V_{max} for each group. This is the volume up to which the fourth brightest galaxy in each group can be detected, which will result in a greater possible volume for the detection of each group. Since the volumes are now underestimated, the number density values are slightly overestimated. However, this effect is likely to be negligible except for very small and nearby groups where the difference in brightness between the fourth and fifth brightest galaxy could be large.

Future work, discussed in Section 5.1, will include a mass-richness relation in the selection function, so that the fitting model will have this incompleteness taken into account.

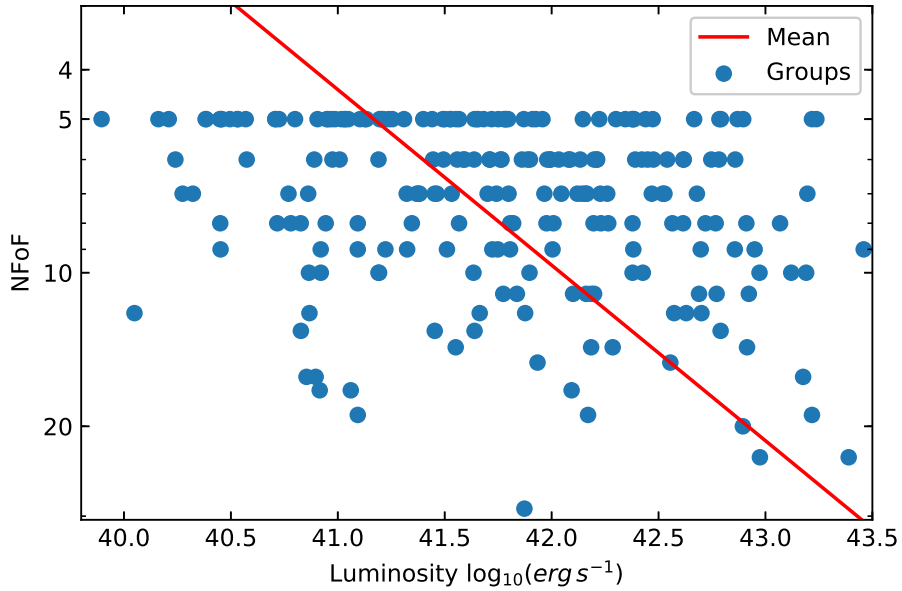

Figure 23: Estimating the relationship between group richness and luminosity by fitting the median values and extrapolating.

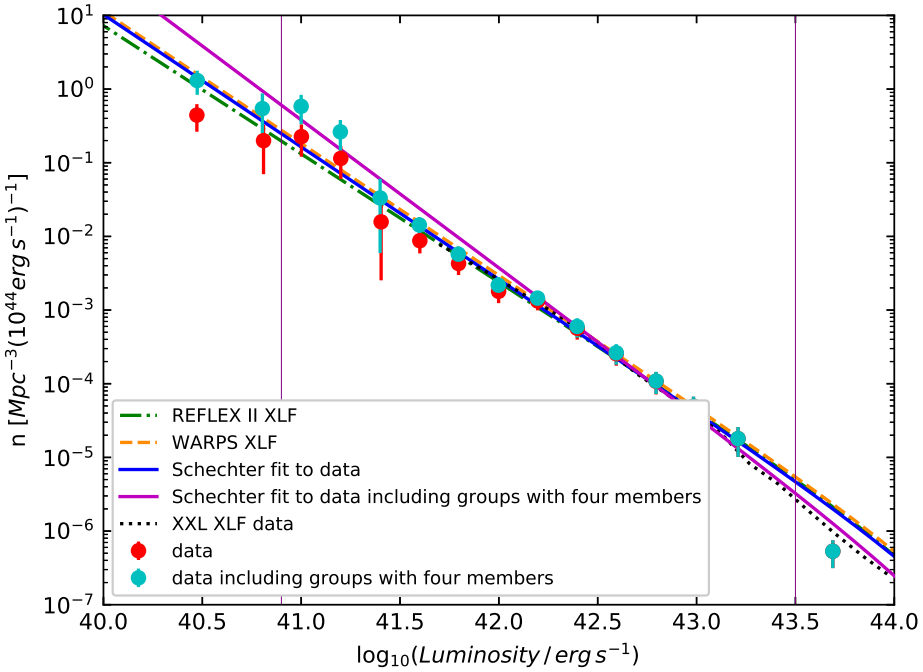

Figure 24: XLF plotted as in Figure 15 overlaid with the data if the luminosities and volumes of groups with four members are estimated and included.

4.5 The number density of low luminosity groups

The XLF shown in Figure 15 shows that the observed number densities of groups with luminosities down to $10^{40.9}$ erg s^{-1} are well explained by a Schechter function. However, the work done by Böhringer, Chon & Collins (2014) found that a Schechter function is not a satisfying analytical description of the REFLEX II XLF since the number of low luminosity groups that they observe is less than expected from a Schechter function, and two other functions are suggested.

The first function is a q-exponential function, as described by Balaguera-Antol\'\inez et al. (2012), which introduces a sharper decrease of the Schechter function at high luminosities. Since this only affects values above L^*, this work is unable to explore its effects, as the sample used does not extend to high enough luminosities.

In order to better constrain the fit for low luminosity groups, the slope of the Schechter function was bent down using a modified function of the form:

$$n(L_x)dL_x = n^* \left(\frac{L_x}{L^*}\right)^{-\alpha} \exp\frac{-L_x}{L^*} \left[1 - \left(1 + \frac{L_x}{\beta}\right)^{-\gamma}\right] \frac{dL_x}{L^*} \tag{22}$$

where $\beta = 10^{43.2}$ erg s^{-1} and $\gamma = 1.7$ are extra parameters whose values where fit separately (Böhringer, Chon & Collins, 2014). This works for the REFLEX II XLF since the minimum luminosity used is $10^{41.3}$ erg s^{-1}, and so the modified Schechter function is a better description of the number densities of groups with luminosities in the range $10^{41.3} - 10^{42.1}$ erg s^{-1} which is lower than that expected from a plain Schechter function for the REFLEX II data.

The galaxy group sample used in this work goes down to far lower luminosities, and even without accounting for the incompleteness, there are low luminosity bins ($10^{41} - 10^{41.3}$ erg s^{-1}) whose number densities are greater than that expected from the best fit Schechter function. For values in the range $10^{41.3} - 10^{42}$ erg s^{-1} the same trend is seen as with the REFLEX II values as the data points all lying below the best fit Schechter function, however, with a first order correction for the incompleteness this is no longer the case, see Figure 24. The implication of this is that the optically selected sample does not show the same deficit once corrected for incompleteness, and so the deficit noted in the REFLEX II data could be related to the X-ray selection.

4.5.1 Surface brightness limitations

While the REFLEX II sample is referred to as flux-limited, it is actually surface brightness limited since the REFLEX II sources are drawn from the RASS source catalogue which uses a sliding cell detection technique. This could result in the X-ray selected sample excluding low-surface brightness groups, which, despite having a high enough flux, are diffuse and as such do not pass the detection threshold. However, the effects of the deficit due to the surface brightness is not estimated by Voges et al. (1999).

The WARPS survey is similarly surface brightness limited, however, the source detection approach used, Voronoi Tessellation and Percolation (VTP), is more efficient at detecting extended sources of low brightness than other methods (Koens et al., 2013). Scharf et al. (1997) goes further to estimate that by using the VTP approach one or two more objects are detected per deg^2 using a flux limit of 3.5×10^{-14} erg s^{-1} cm^{-2} than when using conventional methods. This is a significant number of extra objects detected, and accounts for 6-12% of the objects detected by WARPS. Whilst VTP is far more efficient at detecting low surface brightness sources, it is also missing

even lower surface brightness sources which may have been optically detected but still failed to be detected by VTP.

Due to the large difference in flux limits between the WARPS and REFLEXX II surveys, estimating the number of sources missed by REFLEX II because of not using the VTP approach is non-trivial. However, since the missing objects are due to using a source detection algorithm similar to those compared to by Scharf et al. (1997), the percentage of objects missed should remain consistent, even if the number per deg^2 decreases since there are fewer high luminosity objects. As a first order estimate, the number of REFLEX II objects detected is only 88-94% of the number of objects expected if a detection algorithm which is more optimised for extended sources is used, and so it can be estimated that an order of 300-600 objects are missing, however, this includes many caveats meaning that the actual number missing is far lower. This comparison is very uncertain since the flux limit used is highly different, the comparison by Scharf et al. (1997) was for PSPC fields and not RASS data and the algorithm compared is not the same as the sliding cell detection technique, however, it gives a first order approximation for the number of missing groups. Since roughly 20% of the objects inspected by Böhringer et al. (2013) are identified as groups, it can be estimated that the number of groups missing due to having a low surface brightness is of the order 60-120. However, since these missing objects are all extended objects by definition, they are likely to all be groups, so the upper limit on the number of REFLEX II groups missing due to using the RASS source catalogue detection algorithm is 600.

4.5.2 REFLEX II miss-identifying sources

The fact that REFLEX II observes a decrease in the number density of low luminosity groups may be due to the miss-identification of galaxy groups as AGN, which is more likely to occur for lower luminosity groups. The REFLEX II source identification system inspects 4460 X-ray sources in detail described by Böhringer et al. (2013) for the construction of the REFLEX II sample. 915 groups are identified and the number of groups missing from the sample is estimated by Böhringer et al. (2013) to be of the order of 50, the uncertainty from which is included in the XLF selection function.

Of the sources that where not classified as groups, 30% are classified as AGN and 21% as unidentified sources, meaning that there is no known group or clear and obvious counterpart. Green et al. (2017) analysed a sample of 3470 ROSAT All Sky Survey selected AGN and found that 22 where in fact galaxy groups, often with an AGN residing in the central galaxy. This gives an estimate that 0.6% of AGN are in fact groups that have been miss-classified as AGN, and so it is estimated that the REFLEX II survey has miss-identified roughly seven groups as AGN. Since this is only 0.8% of the sample size, and far fewer than the estimated number of missing groups, its effects can be ignored, and the effects from which are likely covered by the selection function.

4.5.3 Missing groups

An estimation of the number of groups missing from the REFLEX II sample is very difficult to approximate, but has an upper limit of 600. Making any accurate estimations of the effects of these missing groups is difficult without knowing the REFLEX II source detection and identification pipelines in greater detail.

The REFLEX II X-ray luminosity histogram shown in Böhringer, Chon & Collins (2014) compares the observed number of groups compared to the values expected from the best fitting

Schechter function. The Schechter function used to estimate the number of groups in each bin is only fit to luminosity bins above $10^{42.8}$erg s^{-1}. There is an excess of roughly 20 groups detected in the luminosity bin $10^{43.7} - 10^{44}$erg s^{-1}, however, this is less than 2σ and at far higher luminosities than can be found in the GAMA-XXL overlap sample, so is incomparable. When the REFLEX II Schechter function is extrapolated to lower luminosities, a deficit of observed groups emerges. Below $10^{42.8}$ erg s^{-1}, 139 groups are predicted of which only 57 are observed. While this is similar to the observed in Figure 15 for the GAMA-XXL sample, when correcting for incompleteness, as in Figure 24, the deficit in number density is no longer apparent. This indicates that REFLEX II underestimates the number density of low luminosity groups, and the difference noted is consistent with the estimate found by Scharf et al. (1997) for the number of low surface brightness groups which are missing due to the source detection algorithm used.

The WARPS XLF and that determined in this work are in a strong agreement with each other, and the only significant deviation found by Koens et al. (2013) was a significant excess of groups in the luminosity range 1-2$\times10^{43}$erg s^{-1}. Since this work only observed roughly ten groups in this luminosity range it is not possible to make any reasonable comparisons.

5 Summary and conclusions

The overlap between the GAMA optical survey and the XXL X-ray survey creates an exciting opportunity to explore galaxy groups across multiple wavelengths. In this work the X-ray properties of optically selected groups were measured using the XXL X-ray mosaic created by combining multiple *XMM-Newton* observations. Forced X-ray aperture photometry was used, with emission from AGN and other non-group X-ray sources modelled out or removed, and then luminosity posteriors were sampled to deal with non-detections. This sample of galaxy groups were then presented as an X-ray luminosity function (XLF): the number density of groups as a function of X-ray luminosity. The XLF was compared with those from X-ray selected samples, and was found to be in good agreement down to lower-luminosities. The Schechter function best fit parameters observed are consistent with values determined using X-ray selected samples such as those by Koens et al. (2013) and Böhringer, Chon & Collins (2014). The optical selection function used introduces an incompleteness since only groups with five or more members were included in the sample. A first order correction for this was to remove bins from the fit below the X-ray luminosity at which the incompleteness becomes significant. Further work estimated that when including the groups with four members, a Schechter function may no longer be a good description of the number density for lower luminosities as an excess was noted. The issue of incompleteness due to the optical selection function needs to be further explored, and by combining the observed XLF with a theoretical mass function this work will ultimately lead to new constraints on the scaling relation between X-ray luminosity and mass in the galaxy group regime.

5.1 Future work

As galaxy groups are the most powerful cosmological probe available, knowing their properties is key to the study of the 'dark' Universe, that is, dark matter and energy. Estimations of group masses already led to the discovery of dark matter, and being able to further constrain their masses will lead to the ability to further constrain cosmological parameters. Measuring the mass of a group is a non-trivial process, however methods exist, such as using the velocity dispersion of the groups member galaxies to determine its total mass, as done by Robotham et al. (2011). An alternative method is to use gravitational lensing to determine how much mass lies between a distant object, whose shape has been distorted due to the mass's gravitational influence, and the observer. The X-ray luminosity is directly related to the group mass. Therefore, a luminosity - mass relation is of fundamental importance for estimating the masses of groups with limited data quality and for characterising X-ray biases in cosmological studies.

The ultimate goal is to construct a model that predicts the number of groups per luminosity bin, and then computing the Poisson likelihood of the observed number. This model would include interesting astrophysical ingredients starting with a mass function and a luminosity-mass relation to predict the luminosities and a mass-richness relation to predict the richness for the selection function.

5.1.1 X-ray luminosity - mass relation

The X-ray luminosity - mass (LM) relation can be investigated by comparing the observed XLF to that obtained when scaling laws and parameter relations are applied to a mass function. The group mass function will be calculated using the fitting function described by Tinker et al. (2008) and

as calculated by Murray, Power & Robotham (2013). The mass function quantifies the number of dark matter halos per unit mass per unit comoving volume. By setting the redshift range and mass range, the mass function can be integrated in order to obtain the number of expected groups within some redshift and mass range. This number of groups can then be sampled from the mass function in order to create a sample of galaxy groups, each with its own mass and redshift, representative of what is expected in the GAMA-XXL overlap region.

The selection function used in this work is that the fifth brightest member in each group must have an apparent magnitude above -19.8. Using a mass-richness relation, similar to that used by Murata et al. (2018), the richness of each group sampled from the mass function can be estimated. Each group's member galaxies then needs a luminosity, and apparent magnitude, in order to apply the selection function. These luminosities are obtained by sampling from a galaxy luminosity function, similar to that by Loveday et al. (2012), and each group's redshift is used to find their apparent magnitudes. Each group containing five or more members with an apparent magnitude above -19.8 are then kept, and these should represent the groups observed in the GAMA-XXL overlap region. Since these groups were sampled from a mass function, an LM relation is then used to fit the mass function derived group sample to the observed GAMA-XXL group sample.

Using this method the XLF could be refit using a different method where the size of each bin is small enough so that Poisson statistics are used to determine the number of groups in a bin. This will allow the inclusion of bins up to 10^{45} erg s^{-1} with zero detected groups, which, alongside a prior, may allow the fitting of L^*. The primary goal of this is to fix the mass function, which itself is sensitive to cosmology, and to constrain the low luminosity region of the scaling relations. If the data is able to constrain these sufficiently tightly then the possibility of constraining the cosmological parameters will be investigated.

This approach can be translated to the X-ray all-sky survey by eROSITA, combined with future all-sky optical surveys such as LSST to constrain the X-ray properties of galaxy groups and clusters in the limits of high redshift and low mass.

References

Abell G. O., 1958, Astrophysical Journal, Supplement, 3, 211

Adami C. et al., 2018, Astronomy and Astrophysics, 620, A5

Ade P. A. et al., 2016, Astronomy and Astrophysics, 594

Allen S. W., Evrard A. E., Mantz A. B., 2011, Annual Review of Astron and Astrophys, 49, 409

Allen S. W., Schmidt R. W., Fabian A. C., Ebeling H., 2003, Monthly Notices of the RAS, 342, 287

Anderson M. E., Gaspari M., White S. D. M. D., Wang W., Dai X., 2015, Monthly Notices of the RAS, 449, 3806

Assef R. J., Stern D., Noirot G., Jun H. D., Cutri R. M., Eisenhardt P. R. M., 2018, Astrophysical Journal, Supplement, 234, 23

Bahcall N. A., 1979, Astrophysical Journal, 232, 689

Balaguera-Antol\'\inez A., Sánchez A. G., Böhringer H., Collins C., 2012, Monthly Notices of the RAS, 425, 2244

Barkhouse W. A. et al., 2006, Astrophysical Journal, 645, 955

Bertin E., Arnouts S., 1996, Astronomy and Astrophysics, Supplement, 117, 393

Böhringer H., Chon G., Collins C. A. A., Guzzo L., Nowak N., Bobrovskyi S., 2013, Astronomy and Astrophysics, 555, A30

Böhringer H., Chon G., Collins C. A. C. A., 2014, Astronomy and Astrophysics, 570, A31

Böhringer H. et al., 2004, Astronomy & Astrophysics, 425, 367

Burenin R. A., Vikhlinin A., Hornstrup A., Ebeling H., Quintana H., Mescheryakov A., 2007, Astrophysical Journal, Supplement, 172, 561

Chiappetti L. et al., 2018, Astronomy and Astrophysics, 620, A12

Davies L. J. M. et al., 2019, arXiv e-prints

De Martino I., Atrio-Barandela F., 2016, Monthly Notices of the RAS, 461, 3222

de Vaucouleurs G., 1975, in Galaxies and the Universe. Edited by Allan Sandage, Mary Sandage, and Jerome Kristian, with an index prepared by Gustav A. Tammann. Published by the University of Chicago Press (Stars and Stellar Systems. Volume 9), Chicago, IL USA., 1975, p.557, Sandage A., Sandage M., Kristian J., eds., p. 557

Driver S. P. et al., 2011, Monthly Notices of the RAS, 413, 971

Ettori S., Balestra I., 2009, Astronomy and Astrophysics, 496, 343

Faccioli L. et al., 2018, Astronomy and Astrophysics, 620, A9

Felten J. E., Gould R. J., Stein W. A., Woolf N. J., 1966, The Astrophysical Journal, 146, 955

Freeman P., Doe S., Siemiginowska A., 2001, in Proceedings of the SPIE, Vol. 4477, Astronomical Data Analysis, Starck J.-L., Murtagh F. D., eds., pp. 76–87

Giacconi R., Murray S., Gursky H., Kellogg E., Schreier E., Tananbaum H., 1972, Astrophysical Journal, 178, 281

Giles P. A. A. et al., 2016, Astronomy and Astrophysics, 592, A3

Giodini S., Lovisari L., Pointecouteau E., Ettori S., Reiprich T. H., Hoekstra H., 2013, Space Science Reviews, 177, 247

Gladders M. D., Yee H. K. C., 2000, The Astronomical Journal, 120, 2148

Gladders M. D., Yee H. K. C., 2005, Astrophysical Journal, Supplement, 157, 1

Goodman J., Weare J., 2010, Communications in Applied Mathematics and Computational Science, Vol.˜5, No.˜1, p.˜65-80, 2010, 5, 65

Green T. S. et al., 2017, Monthly Notices of the RAS, 465, 4872

Hinshaw G. et al., 2013, The Astrophysical Journal Supplement, 208, 19

Hogg D. W., 1999, arXiv e-prints, astro

Horner D. J., Perlman E. S., Ebeling H., Jones L. R., Scharf C. A., Wegner G., Malkan M., Maughan B., 2008, Astrophysical Journal, Supplement, 176, 374

Huchra J. P., Geller M. J., 1982, Astrophysical Journal, 257, 423

Jones C., Forman W., 1984, Astrophysical Journal, 276, 38

Kaastra J. S. S., Paerels F. B. S. B., Durret F., Schindler S., Richter P., 2008, Space Science Reviews, 134, 155

Kaiser N., 1986, Monthly Notices of the RAS, 222, 323

Koens L. A. A., Maughan B. J. J., Jones L. R. R., Ebeling H., Horner D. J. J., Perlman E. S. S., Phillipps S., Scharf C. A. A., 2013, Monthly Notices of the RAS, 435, 3231

Koester B. P. et al., 2007, Astrophysical Journal, 660, 239

Lieu M. et al., 2016, Astronomy and Astrophysics, 592, A4

Loveday J. et al., 2012, MNRAS, 420, 1239

Lovisari L., Reiprich T. H., Schellenberger G., 2015, Astronomy and Astrophysics, 573, A118

Mantz A., Allen S. W., Ebeling H., Rapetti D., 2008, Monthly Notices of the RAS, 387, 1179

Mantz A. B., 2019, Monthly Notices of the Royal Astronomical Society, 485, 4863

Maughan B. J., 2007, Astrophysical Journal, 668, 772

Mehrtens N. et al., 2012, Monthly Notices of the RAS, 423, 1024

Mohr J. J., Mathiesen B., Evrard A. E., 1999, The Astrophysical Journal, 517, 627

Mullis C. R. et al., 2004, Astrophysical Journal, 607, 175

Murata R., Nishimichi T., Takada M., Miyatake H., Shirasaki M., More S., Takahashi R., Osato K., 2018, Astrophysical Journal, 854, 120

Murray S. G., Power C., Robotham A. S. G., 2013, Astronomy and Computing, 3, 23

Mushotzky R. F., 1984, Physica Scripta Volume T, 7, 157

Pacaud F. et al., 2016, Astronomy and Astrophysics, 592, A2

Pacaud F. et al., 2006, Monthly Notices of the Royal Astronomical Society, 372, 578

Piccinotti G., Mushotzky R. F., Boldt E. A., Holt S. S., Marshall F. E., Serlemitsos P. J., Shafer R. A., 1982, Astrophysical Journal, 253, 485

Pierre M. et al., 2016, Astronomy and Astrophysics, 592, A1

Pratt G. W., Arnaud M., Biviano A., Eckert D., Ettori S., Nagai D., Okabe N., Reiprich T. H., 2019, Space Science Reviews, 215, 25

Primini F. A., Kashyap V. L., 2014, Astrophysical Journal, 796, 24

Read A. M., Rosen S. R., Saxton R. D., Ramirez J., 2011, Astronomy & Astrophysics, 534, A34

Reichardt C. L. et al., 2013, Astrophysical Journal, 763, 127

Robotham A. S. G. et al., 2011, Monthly Notices of the Royal Astronomical Society, 416, 2640

Sarazin C. L., 1986, Rev. Mod. Phys., 58, 1

Scharf C. A., Ebeling H., Perlman E., Malkan M., Wegner G., 1997, Astrophysical Journal, 477, 79

Schechter P., 1976, Astrophysical Journal, 203, 297

Smith R. K. R. K., Brickhouse N. S. N. S., Liedahl D. A. D. A., Raymond J. C. J. C., 2001, The Astrophysical Journal, Letters, 556, L91

Tinker J., Kravtsov A. V., Klypin A., Abazajian K., Warren M., Yepes G., Gottlöber S., Holz D. E., 2008, The Astrophysical Journal, 688, 709

Truemper J., 1993, Science, 260, 1769

Vikhlinin A., McNamara B. R., Forman W., Jones C., Quintana H., Hornstrup A., 1998a, Astrophysical Journal, 502, 558

Vikhlinin A., McNamara B. R., Forman W., Jones C., Quintana H., Hornstrup A., 1998b, Astrophysical Journal, Letters, 498, L21

Vikhlinin A. A., Kravtsov A. V., Markevich M. L., Sunyaev R. A., Churazov E. M., 2014, Physics-Uspekhi, 57, 317

Voges W. et al., 1999, Astronomy and Astrophysics, 349, 389

Wang L. et al., 2014, Monthly Notices of the RAS, 439, 611

White S. D. M., Navarro J. F., Evrard A. E., Frenk C. S., 1993, Nature, 366

Willis J. P. P., Ramos-Ceja M. E. E., Muzzin A., Pacaud F., Yee H. K. C. K., Wilson G., 2018, Monthly Notices of the Royal Astronomical Society, 477, 5517

Yang X., Mo H. J., van den Bosch F. C., Pasquali A., Li C., Barden M., 2007, Astrophysical Journal, 671, 153

Zwicky F., 1933, Helvetica Physica Acta, 6, 110

Zwicky F., Herzog E., Wild P., Karpowicz M., Kowal C. T., 1961, Catalogue of galaxies and of clusters of galaxies, Vol. I

A Luminosities

GroupID	L_X Mode	L_X 95%	L_X Median	L_X 16%	L_X 84%	N_{FoF}	Z	VelDisp	r_c
400001	43.955	43.960	43.955	43.952	43.958	97	.138	660	174
400002	44.069	44.077	44.069	44.064	44.074	59	.184	1120	202
400003	41.972	42.013	41.971	41.945	41.997	54	.053	414	120
400004	43.740	43.778	43.740	43.716	43.763	41	.299	752	213
400007	43.228	43.257	43.227	43.208	43.245	19	.232	655	164
400008	43.381	43.419	43.381	43.356	43.405	23	.301	657	164
400009	42.043	42.238	42.043	41.867	42.173	17	.166	389	92
400010	43.172	43.242	43.173	43.124	43.215	16	.291	663	161
400012	42.974	43.002	42.975	42.956	42.992	23	.137	597	137
400013	42.890	42.915	42.890	42.875	42.906	20	.153	467	117
400014	41.909	42.029	41.910	41.813	41.987	29	.137	337	111
400015	-	41.579	41.116	40.605	41.437	17	.137	476	98
400016	42.532	42.592	42.532	42.491	42.570	15	.194	462	120
400019	40.617	41.478	41.040	40.560	41.338	19	.141	238	68
400020	42.922	42.968	42.922	42.890	42.951	14	.258	407	98
400021	42.785	42.875	42.785	42.720	42.841	13	.289	973	192
400023	42.566	42.634	42.566	42.519	42.608	12	.187	490	99
400025	42.168	42.250	42.168	42.109	42.220	19	.138	277	81
400026	41.754	41.787	41.754	41.733	41.775	42	.054	357	114
400027	42.092	42.210	42.092	42.001	42.167	11	.137	466	124
400028	41.865	41.982	41.865	41.778	41.941	11	.135	251	73
400029	41.901	42.140	41.903	41.652	42.062	12	.210	834	198
400030	-	41.892	41.426	40.898	41.746	13	.277	745	113
400031	40.863	40.936	40.863	40.811	40.909	16	.053	152	53
400032	41.665	41.893	41.666	41.443	41.818	12	.208	284	101
400033	42.972	43.033	42.971	42.930	43.009	10	.307	561	161
400034	41.507	42.172	41.758	41.282	42.043	10	.292	359	122
400035	42.704	42.807	42.703	42.626	42.769	11	.306	693	138
400036	42.310	42.467	42.311	42.180	42.412	14	.234	394	116
400037	41.223	41.438	41.226	41.019	41.364	10	.158	245	75
400039	40.679	41.191	40.815	40.360	41.066	17	.142	225	88
400040	42.708	42.807	42.708	42.635	42.770	12	.276	567	161
400041	-	40.521	40.051	39.544	40.373	32	.070	284	111
400042	42.763	42.846	42.764	42.706	42.815	11	.275	218	67
400043	40.401	41.143	40.723	40.238	41.010	12	.152	371	108
400045	43.550	43.582	43.549	43.528	43.569	11	.347	1024	219
400046	40.681	41.107	40.759	40.345	40.996	13	.070	256	87
400047	43.127	43.171	43.127	43.099	43.154	10	.253	306	105
400048	-	41.115	40.655	40.133	40.967	16	.106	146	53
400049	42.209	42.288	42.209	42.152	42.259	11	.263	362	84
400050	43.157	43.290	43.188	43.130	43.250	10	.291	556	172

Table A1 continued from previous page

GroupID	L_X Mode	L_X 95%	L_X Median	L_X 16%	L_X 84%	N_{FoF}	Z	VelDisp	r_c
400051	42.189	42.282	42.189	42.120	42.248	11	.139	351	80
400053	40.389	41.601	41.157	40.634	41.461	10	.243	641	135
400054	41.726	41.754	41.726	41.708	41.743	9	.083	306	66
400055	41.468	41.992	41.615	41.163	41.872	14	.257	418	141
400056	43.452	43.519	43.452	43.407	43.493	9	.446	1256	308
400059	42.785	42.854	42.785	42.738	42.827	8	.254	610	128
400060	41.999	42.126	41.999	41.902	42.079	8	.137	202	69
400061	-	41.325	40.860	40.332	41.178	10	.137	266	79
400062	-	40.781	40.321	39.782	40.641	9	.070	152	62
400064	40.098	41.071	40.619	40.111	40.925	8	.075	274	70
400065	42.432	42.565	42.432	42.328	42.517	10	.232	346	118
400066	41.506	41.564	41.507	41.467	41.542	9	.042	88	33
400068	42.572	42.704	42.570	42.466	42.657	8	.316	343	92
400069	41.475	41.627	41.476	41.357	41.571	13	.150	320	94
400070	-	41.459	40.993	40.458	41.313	9	.263	368	118
400072	42.691	42.763	42.692	42.641	42.736	8	.315	470	107
400073	42.404	42.468	42.405	42.362	42.444	9	.141	355	88
400074	42.002	42.169	42.004	41.858	42.111	8	.217	361	83
400075	42.270	42.377	42.271	42.185	42.339	8	.179	488	133
400076	42.200	42.349	42.201	42.080	42.295	14	.182	268	112
400078	41.628	41.715	41.629	41.569	41.683	10	.087	222	73
400079	41.804	41.868	41.804	41.759	41.845	8	.139	490	145
400080	-	40.581	40.119	39.580	40.435	12	.080	300	100
400081	42.188	42.255	42.189	42.144	42.230	11	.172	396	94
400083	-	40.635	40.169	39.631	40.488	7	.084	118	52
400085	42.141	42.363	42.145	41.928	42.289	7	.285	318	85
400086	-	42.117	41.661	41.155	41.976	7	.252	411	74
400087	-	41.677	41.215	40.701	41.530	9	.205	164	57
400088	40.839	41.582	41.160	40.680	41.448	7	.181	297	73
400090	42.599	42.918	42.618	42.280	42.818	7	.439	221	100
400094	40.375	41.961	41.501	40.964	41.816	7	.197	129	51
400096	42.142	42.269	42.141	42.041	42.223	7	.231	247	71
400097	42.588	42.719	42.588	42.481	42.671	12	.291	320	108
400098	42.516	42.525	42.516	42.510	42.521	7	.198	198	64
400099	-	41.375	40.912	40.385	41.225	8	.198	463	83
400101	42.915	42.981	42.916	42.869	42.956	8	.231	246	82
400102	42.023	42.235	42.025	41.818	42.162	9	.307	292	112
400103	40.432	41.362	40.916	40.406	41.228	8	.209	501	113
400106	42.692	42.742	42.692	42.658	42.723	9	.190	278	70
400107	42.263	42.418	42.264	42.136	42.364	7	.195	116	36
400108	43.068	43.102	43.068	43.046	43.089	8	.297	497	154
400109	42.896	42.983	42.896	42.834	42.950	9	.294	687	146

Table A1 continued from previous page

GroupID	L_X Mode	L_X 95%	L_X Median	L_X 16%	L_X 84%	N_{FoF}	Z	VelDisp	r_c
400113	42.401	42.526	42.402	42.303	42.479	10	.182	585	119
400114	41.253	42.200	41.766	41.259	42.063	9	.222	269	84
400115	40.435	40.527	40.435	40.369	40.493	8	.034	175	55
400116	41.469	41.642	41.466	41.305	41.582	7	.133	347	66
400118	41.988	42.147	41.986	41.856	42.088	15	.291	527	175
400119	43.189	43.211	43.189	43.176	43.202	7	.263	615	148
400122	41.530	41.656	41.529	41.426	41.610	6	.091	107	31
400123	41.659	41.865	41.658	41.458	41.795	6	.148	180	64
400124	42.852	42.910	42.852	42.813	42.888	6	.280	431	147
400125	-	41.334	40.872	40.355	41.190	6	.143	88	36
400127	-	41.799	41.342	40.814	41.655	6	.220	163	56
400128	-	41.234	40.770	40.247	41.085	7	.137	298	72
400129	41.132	41.669	41.285	40.834	41.548	8	.178	214	69
400130	40.894	41.119	40.900	40.678	41.045	6	.072	239	49
400131	-	41.710	41.257	40.738	41.574	9	.215	225	91
400133	42.289	42.487	42.292	42.099	42.420	6	.298	258	85
400134	-	41.452	40.990	40.468	41.307	9	.137	359	103
400135	42.620	42.688	42.619	42.573	42.662	6	.209	389	100
400137	42.572	42.730	42.574	42.445	42.674	6	.179	264	47
400138	42.197	42.272	42.197	42.144	42.244	6	.210	222	52
400139	42.506	42.675	42.507	42.362	42.613	7	.313	609	187
400140	-	42.111	41.647	41.128	41.967	6	.317	297	74
400141	42.343	42.502	42.340	42.209	42.445	6	.295	512	112
400142	40.858	40.914	40.858	40.818	40.893	10	.053	113	53
400143	42.785	42.837	42.785	42.750	42.818	6	.345	634	197
400144	42.106	42.272	42.110	41.968	42.214	6	.211	316	86
400145	41.822	42.173	41.854	41.485	42.075	6	.269	282	84
400146	42.166	42.320	42.164	42.035	42.265	6	.207	318	65
400150	-	41.763	41.293	40.792	41.614	7	.205	245	76
400151	42.045	42.188	42.043	41.926	42.137	7	.189	117	46
400152	41.913	42.264	41.947	41.588	42.160	6	.252	315	69
400153	41.808	41.894	41.809	41.747	41.863	9	.151	215	70
400155	42.509	42.626	42.511	42.424	42.585	7	.237	539	85
400156	42.279	42.340	42.279	42.236	42.317	7	.156	551	90
400160	-	41.142	40.685	40.153	41.006	7	.152	415	122
400161	41.546	41.654	41.546	41.465	41.615	6	.151	305	81
400162	42.185	42.237	42.185	42.150	42.218	7	.198	277	97
400163	-	40.169	39.697	39.178	40.012	6	.044	88	36
400164	42.921	42.948	42.921	42.904	42.937	11	.140	276	99
400165	41.492	41.908	41.560	41.154	41.799	7	.207	489	130
400168	40.909	41.237	40.936	40.585	41.145	5	.083	122	43
400169	42.893	43.037	42.894	42.776	42.986	5	.248	77	24

Table A1 continued from previous page

GroupID	L_X Mode	L_X 95%	L_X Median	L_X 16%	L_X 84%	N_{FoF}	Z	VelDisp	r_c
400170	42.756	42.886	42.755	42.647	42.841	5	.341	377	101
400171	-	41.668	41.210	40.697	41.526	5	.291	280	60
400172	-	41.029	40.559	40.041	40.886	5	.152	290	69
400173	42.375	42.419	42.374	42.344	42.402	5	.203	377	97
400174	-	41.972	41.510	40.987	41.831	5	.288	294	96
400175	-	42.083	41.624	41.088	41.939	11	.293	591	146
400176	42.544	42.672	42.543	42.442	42.626	8	.304	966	214
400177	43.226	43.277	43.226	43.191	43.258	5	.444	748	145
400178	41.035	41.130	41.034	40.966	41.094	5	.042	39	12
400179	-	41.299	40.839	40.308	41.159	6	.132	498	161
400180	-	41.576	41.114	40.594	41.428	5	.196	425	88
400181	41.982	42.158	41.982	41.826	42.096	6	.178	209	63
400183	42.470	42.606	42.471	42.363	42.557	6	.280	208	68
400184	-	40.712	40.249	39.734	40.566	7	.070	172	77
400185	-	40.606	40.143	39.632	40.459	5	.070	262	66
400186	-	41.057	40.589	40.052	40.909	5	.072	95	27
400187	42.184	42.258	42.183	42.133	42.230	8	.139	315	101
400188	-	41.471	41.010	40.475	41.326	5	.134	595	204
400189	40.176	41.316	40.859	40.360	41.175	5	.134	249	70
400192	41.765	42.058	41.776	41.468	41.967	5	.195	304	56
400193	40.544	40.670	40.544	40.447	40.622	6	.135	119	54
400194	-	41.583	41.112	40.576	41.438	7	.160	129	54
400195	41.664	42.104	41.747	41.319	41.990	5	.238	233	77
400196	40.899	41.925	41.470	40.951	41.784	5	.240	188	60
400197	41.986	42.173	41.986	41.812	42.108	6	.205	769	190
400199	41.504	41.729	41.503	41.267	41.655	5	.130	232	64
400200	41.180	42.055	41.618	41.110	41.913	5	.214	232	75
400201	41.766	42.069	41.781	41.464	41.975	7	.194	397	98
400203	-	41.501	41.033	40.517	41.360	5	.189	388	68
400204	41.507	42.169	41.760	41.287	42.038	5	.331	633	192
400205	42.613	42.729	42.612	42.524	42.686	6	.231	347	92
400206	41.798	42.050	41.803	41.549	41.969	5	.232	315	84
400207	41.928	42.160	41.933	41.700	42.084	7	.197	229	71
400208	41.860	42.015	41.859	41.728	41.960	6	.197	276	73
400212	-	41.012	40.551	40.017	40.870	5	.139	142	45
400213	41.225	41.261	41.225	41.202	41.248	5	.068	70	34
400214	41.750	41.863	41.750	41.659	41.823	5	.182	164	50
400215	41.683	41.775	41.684	41.614	41.742	5	.139	303	41
400217	41.395	41.660	41.401	41.121	41.576	5	.227	238	63
400218	41.851	42.082	41.855	41.624	42.007	5	.292	202	65
400219	40.598	41.173	40.774	40.315	41.048	5	.143	328	97
400220	41.270	41.575	41.284	40.969	41.478	5	.208	204	60

Table A1 continued from previous page

GroupID	L_X Mode	L_X 95%	L_X Median	L_X 16%	L_X 84%	N_{FoF}	Z	VelDisp	r_c
400221	42.951	42.965	42.951	42.943	42.960	9	.142	385	113
400223	42.426	42.620	42.425	42.245	42.554	6	.299	331	91
400224	41.748	41.993	41.749	41.494	41.913	5	.175	208	70
400225	42.297	42.473	42.299	42.142	42.414	5	.298	441	122
400226	-	41.403	40.948	40.412	41.264	8	.144	221	74
400227	-	41.910	41.443	40.918	41.764	5	.277	316	111
400228	41.752	42.151	41.809	41.397	42.042	5	.232	88	36
400229	40.744	40.965	40.745	40.531	40.893	5	.044	46	21
400230	42.190	42.397	42.190	41.988	42.328	5	.265	556	159
400231	43.231	43.285	43.231	43.195	43.264	5	.431	536	124
400232	42.098	42.171	42.098	42.047	42.144	6	.139	222	65
400233	-	41.808	41.348	40.817	41.664	5	.205	314	75
400234	41.623	42.103	41.730	41.282	41.988	6	.185	459	105
400235	41.777	41.983	41.779	41.583	41.914	8	.139	255	82
400236	42.732	42.805	42.731	42.680	42.777	6	.278	444	116
400237	42.321	42.436	42.321	42.235	42.393	5	.203	179	52
400238	42.442	42.551	42.444	42.365	42.509	5	.188	102	51
400239	41.821	41.990	41.818	41.666	41.931	5	.179	284	90
400240	-	41.478	41.011	40.506	41.332	6	.183	417	104
400242	-	40.362	39.883	39.371	40.212	5	.043	174	76
400244	41.189	41.334	41.189	41.073	41.281	5	.041	92	25
400245	41.653	41.807	41.652	41.524	41.752	5	.137	455	101
400249	41.156	41.358	41.156	40.969	41.289	5	.070	73	23
400250	42.661	42.814	42.661	42.534	42.760	5	.297	487	123
400251	40.284	40.691	40.345	39.939	40.573	5	.042	123	52
400252	-	41.496	41.035	40.497	41.352	5	.137	171	55
400253	-	40.723	40.259	39.740	40.572	5	.056	127	33
400258	42.259	42.372	42.259	42.175	42.332	5	.297	443	129
400260	40.164	40.448	40.176	39.873	40.358	6	.030	155	49
400261	-	40.810	40.352	39.824	40.665	5	.079	188	50
400262	42.842	42.979	42.841	42.734	42.930	5	.402	287	98
400263	42.489	42.611	42.488	42.394	42.567	5	.298	494	147
400271	-	42.171	41.697	41.176	42.023	7	.380	431	171
400275	-	40.719	40.252	39.741	40.573	5	.097	179	56
400282	-	41.124	40.660	40.132	40.981	8	.154	376	85
400294	42.799	42.974	42.801	42.647	42.914	5	.450	660	241
400298	-	42.239	41.782	41.248	42.095	5	.352	380	117
400300	-	41.133	40.679	40.161	40.995	5	.157	354	107
400305	41.997	42.340	42.025	41.666	42.237	6	.237	244	68
400308	-	41.400	40.923	40.399	41.251	5	.137	133	50
400310	42.170	42.317	42.170	42.046	42.268	5	.216	183	69
400325	41.616	41.787	41.615	41.465	41.728	6	.130	272	73

Table A1 continued from previous page

GroupID	L_X Mode	L_X 95%	L_X Median	L_X 16%	L_X 84%	N_{FoF}	Z	VelDisp	r_c
400329	-	41.375	40.913	40.386	41.230	5	.137	243	71
400334	-	41.328	40.875	40.340	41.180	5	.138	158	58
400360	-	41.616	41.151	40.604	41.466	7	.277	533	144
400361	41.763	41.979	41.763	41.544	41.907	6	.277	149	78
400365	-	40.989	40.517	39.996	40.844	5	.149	269	80
400367	42.228	42.339	42.228	42.149	42.298	8	.324	656	184
400371	41.895	42.078	41.895	41.725	42.017	6	.255	120	53
400377	42.698	42.819	42.697	42.606	42.775	7	.294	249	106
400381	40.460	41.383	40.943	40.449	41.247	5	.140	389	99
400385	-	41.087	40.628	40.093	40.942	5	.150	251	74
400386	42.372	42.464	42.372	42.306	42.431	8	.320	343	126
400389	-	40.651	40.186	39.658	40.509	5	.085	259	66
400393	-	41.377	40.916	40.397	41.233	5	.219	179	61
400399	-	42.048	41.582	41.070	41.900	6	.279	213	70
400401	42.106	42.341	42.109	41.872	42.264	7	.290	704	137
400414	-	42.211	41.751	41.230	42.064	5	.216	67	28
400423	42.015	42.367	42.049	41.686	42.265	6	.334	238	88
400424	-	41.502	41.044	40.530	41.359	5	.185	278	91
400430	41.175	41.262	41.175	41.112	41.230	5	.043	58	28
400432	42.429	42.535	42.430	42.350	42.498	6	.236	526	110
400443	-	41.810	41.341	40.813	41.661	6	.193	131	58
400459	-	41.905	41.440	40.927	41.764	5	.176	54	28
400463	41.415	42.367	41.926	41.413	42.227	8	.333	505	178
400672	40.604	41.857	41.412	40.901	41.717	5	.179	396	95
400762	42.420	42.585	42.420	42.277	42.527	5	.318	202	86

Table A1: X-ray luminosities of the optically selected GAMA-XXL group sample determined from each groups luminosity prior, given in units $\log_{10}(\text{Luminosity/erg s}^{-1})$. Also given is each groups richness ($N_{\rm FoF}$), velocity dispersion(in units of km s^{-1}) and core radius (r_c, in units of kpc).

B Markov Chain Monte Carlo

Markov Chain Monte Carlo (MCMC) methods are used to sample multi-dimensional probability distributions proportional to a known function. MCMC works by taking a starting 'guess' value for each parameter, finding the probability of this value using a defined probability distribution, and then proposing a random step. The probability of this next step is then found, and if if this is higher than the current steps probability, it will be taken. If not, the ratio of the probabilities is found, and a random number between 0 and 1 created If the random number is smaller than the ratio, the step is taken anyway, else the step is cancelled. The chain then walks through possible values, spending more time in areas of higher probability, but exploring all parameter space.

Since the chain is started by a guess, it will spend some time before spreading out across parameter space, and as such the initial values in the chains, the burn-in phase, are removed. The length of the burn-in can be found by looking at the probability produced at each step for each

walker, with the burn-in phase values having a considerably lower probability than later values. Since the chains are randomly walking through the parameter space, they may spend some time being stuck at certain values. To combat this the resulting chains can be thinned where every nth (e.g. 5th) value is kept and the rest removed.

This work incorporates an affine invariant MCMC algorithm package for python called EMCEE, based on Goodman & Weare (2010).